Tectonophysics 744 (2018) 458–483

Contents lists available at ScienceDirect

Tectonophysics

journal homepage: www.elsevier.com/locate/tecto

Age and setting of Permian Slide Mountain terrane ophiolitic ultramafic-mafic complexes in the Yukon: Implications for late Paleozoic-early Mesozoic tectonic models in the northern Canadian Cordillera

Cees R. van Staal[a,b,*], Alexandre Zagorevski[c], William C. McClelland[d], Monica P. Escayola[e], James J. Ryan[a], Andrew J. Parsons[a,f], Joaquin Proenza[g]

[a] Geological Survey of Canada, 1500-605 Robson Street, Vancouver, BC V6B 5J3, Canada
[b] Dept. Earth and Environmental Sciences, University of Waterloo, ON N2L 3G1, Canada
[c] Geological Survey of Canada, 601 Booth St., Ottawa, ON K1A 0E8, Canada
[d] Dept. Earth and Environmental Sciences, 115 Trowbridge Hall, University of Iowa, Iowa City, IA 52242, USA
[e] Instituto de Ciencias Polares y Ambientales ICPA, Universidad de Tierra del Fuego-CONICET, Fueguia Basket 251, 9410 Ushuaia, Tierra del Fuego, Argentina
[f] Department of Earth Sciences, Oxford University, Parks Road, Oxford 0X1 3PR, UK
[g] Departament de Cristallografia, Mineralogia i Dipòsits Minerals, Universitat de Barcelona, C/Martí i Franquès, s/n, 08028 Barcelona, Spain

ARTICLE INFO

Keywords:
Cordillera
Suprasubduction zone ophiolites
Klondike orogeny
Slide Mountain terrane
Yukon Tanana terrane

ABSTRACT

The Yukon Tanana (YTT) and Slide Mountain terranes (SMT) of the Cordillera in Canada and Alaska were interpreted in terms of opening and closing of a Late Devonian-Permian Japan Sea-style backarc basin behind a continental arc built upon YTT, which rifted from Laurentia during the Famennian-early Mississippian. Formation of Famennian transitional oceanic lithosphere supports rifting, but a combination of existing and new data on the setting and age of SMT ophiolites do not support the Japan Sea model.

The studied Clinton Creek and Midnight Dome complexes represent suprasubduction zone ophiolites formed at ca. 265 Ma, consistent with analyses of other SMT ophiolites. Ultramafic rocks dominate most ophiolites. They lack sheeted dikes and contain relatively minor volumes of mafic plutonic and volcanic rocks, suggesting they formed in oceanic core complexes characterised by slow spreading and low magma productivity. The Permian ophiolites formed during or immediately after eclogite formation in YTT, coeval with or immediately preceding emplacement of orogenic peridotites into YTT due to hyperextension. Several tectonic scenarios are discussed. We propose that YTT is a composite terrane comprising a continental block and an oceanic arc-backarc complex with the latter obducted onto the former during the middle Permian-early Triassic Klondike orogeny. Obduction may have come from the west or east, but east-directed obduction is most consistent with geological constraints. Obduction was followed by initiation of west-dipping subduction east of the composite YTT; slab roll back causing extension in the composite upper plate, leading to exhumation of orogenic peridotites. Tectonic relationships show many analogies to the collision between Australia and the New Britain arc, in which collision in the Huon Peninsula of New Guinea is contemporaneous with extension in Australian crust in the adjacent Woodlark basin. Syn-orogenic Permian Klondike calc-alkaline magmatism is attributed to extension in a Woodlark basin-like setting rather than a representing a continental arc.

1. Introduction

The Northern Cordillera in Canada and Alaska is thought to preserve evidence of opening and closing of the Late Devonian-Permian Slide Mountain Ocean (SMO). Late Permian closure of this oceanic basin is generally interpreted to have resulted in collision of the western Laurentian passive margin with the Yukon-Tanana terrane (YTT; Colpron et al., 2006b) following the Permian Klondike arc cycle. This model of arc-continent collision, which returned the YTT to its ancestral place of origin along northwestern Laurentia, is generally referred as the Klondike orogeny in Canada (Mortensen, 1992; Beranek and Mortensen, 2011). However, evidence for this collision is enigmatic and is opposite to what is expected in an arc-continent collision (e.g. Brown et al., 2011). That is the passive margin of western Laurentia

* Corresponding author at: Geological Survey of Canada, 1500-605 Robson Street, Vancouver, BC V6B 5J3, Canada.
E-mail address: cees.vanstaal@canada.ca (C.R. van Staal).

https://doi.org/10.1016/j.tecto.2018.07.008
Received 10 April 2018; Received in revised form 2 July 2018; Accepted 10 July 2018
Available online 18 July 2018

(downgoing plate) preserves little structural and sedimentological evidence for the Klondike orogeny (Gordey et al., 1991; Gordey, 2002), whereas Permian orogenesis and metamorphism is widespread in the YTT, the upper plate in this scenario (Berman et al., 2007; Beranek and Mortensen, 2011; Petrie et al., 2015). Numerous ultramafic-mafic massifs and associated marine sedimentary rocks are exposed *along* the suture zone and as structural outliers above the YTT. Most of these rocks were previously grouped into the Slide Mountain terrane (SMT) and are generally considered to represent vestiges of the SMO, which is considered to represent an extension of the Anvil (Tempelman-Kluit, 1979) or Angayucham oceans further to the north (e.g., Nelson, 1993; Nelson et al., 2006; Plint and Gordon, 1997). Many workers have interpreted these ultramafic-mafic massifs as components of structurally dismembered ophiolites (e.g., Foster and Keith, 1974; Nelson, 1993; Roback et al., 1994; Dusel-Bacon et al., 2006; Dusel-Bacon et al., 2013; Parsons et al., 2018a) that formed during separation of the YTT from North America and opening of the SMO backarc basin (e.g., Mortensen, 1992; Creaser et al., 1997a, 1999; Colpron et al., 2006b; Nelson et al., 2013). These ophiolites represent a crucial, yet enigmatic tectonic element of the SMO in Alaska, Yukon and British Columbia because they are interpreted to have formed part of the upper plate during departure of the YTT from Laurentia and protracted opening of the SMO, subsequently becoming part of the subducting plate during closure of the SMO and yet were obducted onto YTT and Laurentia during the terminal Permian collision.

Understanding the origin and tectonic setting of the ultramafic-mafic complexes currently assigned to SMT and YTT is of fundamental importance to understanding the Paleozoic-Mesozoic tectonic evolution of the northern Cordillera; yet their ages and chemical characteristics are generally poorly known. Hence, the timing and tectonic setting of ophiolite formation, which has a profound influence on interpretation of the mafic-ultramafic complexes and their ultimate emplacement mechanisms, are unclear. In this paper, we examine the relatively well preserved mafic-ultramafic complexes at Clinton Creek, Midnight Dome and the St. Cyr klippe in western Yukon, which are generally interpreted as correlatives of the SMT (Colpron et al., 2016). We present new geochemical and geochronological data, discuss their tectonic setting and compare these mafic-ultramafic complexes to broadly coeval rocks elsewhere in the northern Cordillera. We demonstrate that extant and herein presented data indicate that the current terrane concept and tectonic models require revision and propose that the suprasubduction zone (SSZ) ophiolitic rocks of the SMT formed in the Panthalassa Ocean, outboard of YTT, rather than in the marginal basin referred to as the SMO. We discuss several tectonic scenarios that are based on modern and ancient analogues to explain the observed characteristics and propose that the term SMO should be abandoned.

2. Geological setting and existing tectonic models

Paleozoic tectonic evolution of the Intermontane belt of the Canadian Cordillera (Fig. 1) is commonly interpreted in terms of development, departure and re-accretion of an episodic Late Devonian-late Permian continental arc, remnants of which are now preserved in the YTT (e.g., Mortensen, 1992; Creaser et al., 1997a, 1997b; Colpron et al., 2006a, 2006b; Colpron et al., 2007; Pecha et al., 2016 and references therein). This Paleozoic arc is inferred to have been built upon the leading Panthalassan (proto-Pacific) edge of Laurentia and developed above an east-dipping subduction zone. Most of the YTT is complexly deformed and metamorphosed (e.g. Tempelman-Kluit, 1979; Berman et al., 2007; Staples et al., 2016) making primary tectonostratigraphic relationships difficult to establish. Correlative rocks in the YTT of southeast Alaska have a similar Laurentian provenance. However, arc magmatism may have initiated there much earlier in the Late Ordovician (e.g. Endicott Arm assemblage, Fig. 1) (Gehrels et al., 1992; Pecha et al., 2016).

The YTT is underlain by Devonian, and older predominantly siliciclastic sedimentary basement, which is generally referred to as the Snowcap assemblage in the Yukon (Colpron et al., 2006a, 2007). Detrital zircon and isotopic provenance studies indicate that the Snowcap assemblage has a continental, Laurentian detrital source (Piercey and Colpron, 2009 and references therein), however the basement to the siliciclastic rocks is not exposed. Isotopic, geochemical and inheritance data from middle Paleozoic felsic intrusive rocks also support presence of Laurentian continental crust below most (but not necessarily all – see below) of the Snowcap assemblage (Piercey et al., 2003; Murphy et al., 2006; Piercey et al., 2006; Ruks et al., 2006 and references therein).

Late Devonian magmatism in the Laurentian margin and YTT is generally interpreted to indicate east-directed subduction beneath the Panthalassan margin of Laurentia, which resulted in Famennian-Mississippian rifting of the YTT from Laurentia and opening of the SMO in a backarc setting. The remnants of the SMO are thought to be preserved in the SMT (Colpron et al., 2006b, 2007), which is mainly situated in a belt and isolated allochthons near the eastern edge of the YTT and on Laurentia.

Backarc spreading progressively moved and isolated the YTT arc terrane(s) from the ancestral Panthalassan margin of Laurentia (Harms and Murchey, 1992; Nelson, 1993; Stevens et al., 1996; Piercey et al., 2004). YTT in these models thus differs from its Laurentian parent by principally displaying post-Famennian magmatism, whereas the remaining autochthonous edge of Laurentia was situated farthest inboard and became the passive margin to the SMO. These models propose that subsequent subduction initiation in the SMO led to its middle-late Permian closure and re-assembly of the YTT, SMT and Laurentia (Mortensen, 1992; Nelson et al., 2006; Murphy et al., 2006; Colpron et al., 2006a, 2006b, 2007). The resultant deformation, metamorphism and concomitant magmatism resulted in the Klondike orogeny in Yukon (Beranek and Mortensen, 2011).

The width of the SMO during the Permian is largely unconstrained. Some workers proposed a width of several thousand kilometers (Belasky et al., 2002, 2006; Nelson et al., 2006, 2013), whereas others suggested a narrow marginal oceanic seaway (Nelson, 1993; Creaser et al., 1997a, 1999; Piercey et al., 2012). Since the YTT is generally inferred to have returned to approximately its place of origin (Nelson et al., 2006; Pecha et al., 2016), this requires that either the divergence and convergence vectors during its opening and closing to have been broadly coincident or that Mesozoic rearrangement of terranes resulted in virtually no net displacements parallel to the Panthalassan Laurentian margin. If correct, this would support a narrow seaway rather than a wide ocean. On the other hand, faunal data such as the Permian McCloud fusilinid fauna in the SMT and YTT and paleomagnetism recorded in red chert units of SMT suggest that these terranes were possibly as far south as Texas during the Permian (Ross, 1969; Richards et al., 1993), hence requiring large successive southward and northward margin-parallel translations of surprisingly similar magnitude (Nelson et al., 2006).

This model of YTT-SMT-North America evolution is widely accepted, yet, existing geological data and tectonic considerations raise questions or require special conditions with respect to its underlying assumptions. These include (i) a causative mechanism for initiation of subduction in the SMO, (ii) development of eclogite within the upper plate YTT (Gilotti et al., 2017), (iii) detachment and obduction of the SMT ophiolites while forming part of the downgoing plate. We will examine each of these issues in greater detail below.

(i) Established tectonic models do not adequately explain the cause of subduction flip from east-dipping subduction in Panthalassa to initiation of west-dipping subduction in the SMO backarc following as much as 70 my of continuous or discontinuous backarc spreading. Berman et al. (2007) suggested that the west-facing YTT arc “overtook rollback” such that the upper plate YTT velocity was greater than trench retreat, resulting in intra-arc shortening, subduction flip and initiation of west-dipping subduction in the SMO

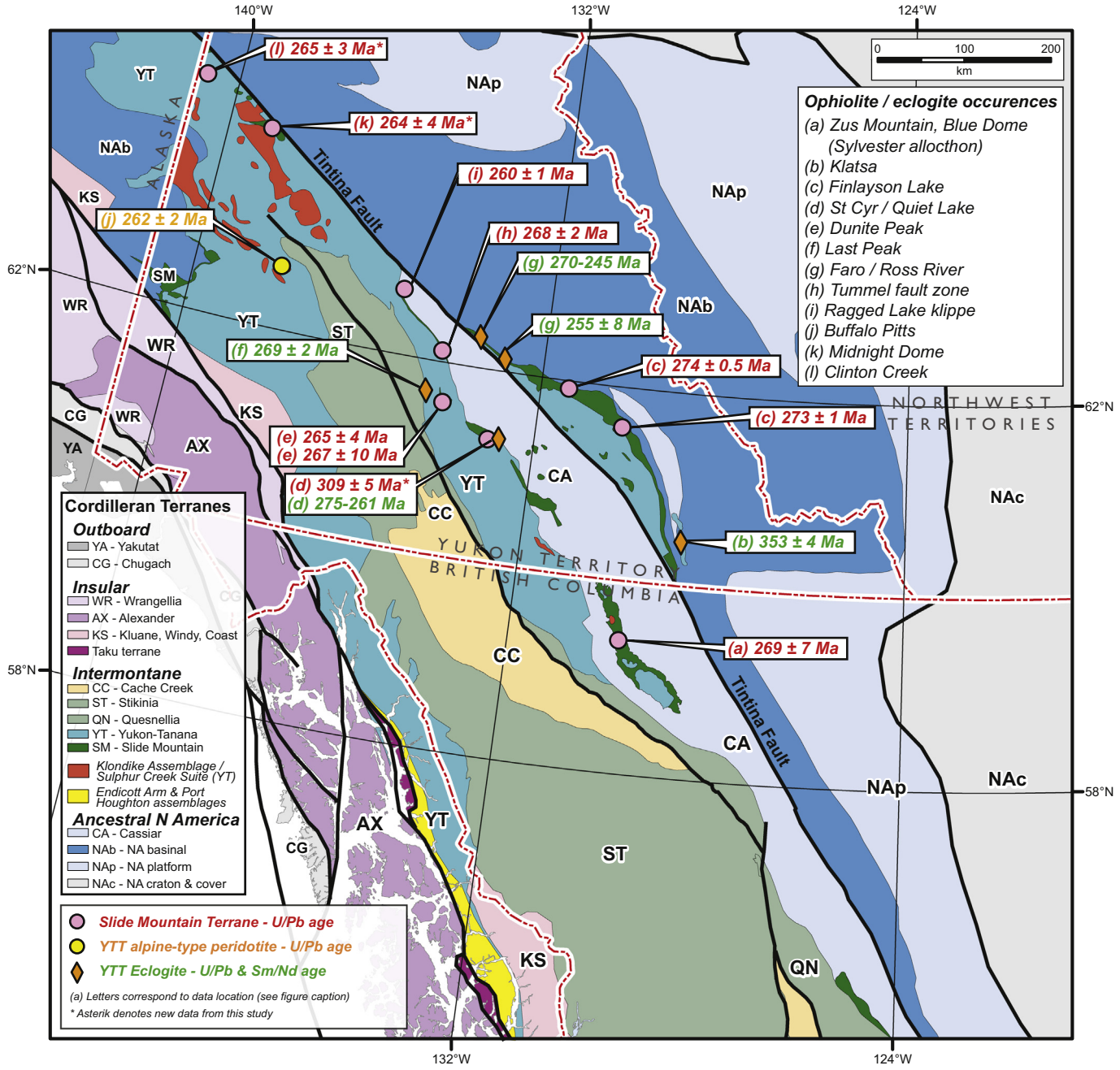

Fig. 1. Distribution of the Slide Mountain and Yukon-Tanana terranes in the northern Cordillera.
(After Colpron and Nelson, 2011; Colpron et al., 2016; Pecha et al., 2016 and Parsons et al., 2018a). Ages from Htoon, 1981; Erdmer and Armstrong (1988); Mortensen (1992); Gabrielse et al. (1993); Oliver (1996); Creaser et al. (1997a, 1997b); Erdmer et al. (1998); Fallas et al. (1998); Goodwin-Bell (1998); De Keijzer et al. (2000); Philippot et al. (2001); Breitsprecher and Mortensen (2004); Colpron et al. (2005, 2006a, 2006b); Murphy et al. (2006); Berman et al. (2007); Staples et al. (2014); Joyce et al. (2015); Petrie et al. (2015, 2016); Gilotti et al. (2017); Parsons et al. (2018a) and this paper.)

(Fig. 2). This scenario does not appear to have modern analogues, because modern subduction zones that are not proximal to a collision zone and have higher upper plate velocities than trench retreat are not associated with subduction flips (e.g., Aleutians: Lallemand et al., 2005). Recent examples of subduction flip or step-back in the southwest Pacific have generally resulted from a collision (e.g., Hall, 2002). For example, the subduction initiation along the southern Philippine and Cotabato trenches can be, in-part, attributed to the closure of the Molucca Sea and collision of Halmahera and Sangihe arcs (see Fig. 2 in Sajona et al., 2000), whereas subduction initiation along the San Cristobal trench was caused by Solomon arc – Ontong Java plateau collision (e.g., Taira et al., 2004). As such, termination and reversal of Panthalassan subduction and initiation of SMO subduction seem to require a collider that has not been identified in the established models, although potential candidates may be hidden in the composite YTT.

(ii) Established tectono-stratigraphic relationships between various components of the YTT indicate that they have undergone episodic magmatism, crustal shortening, deformation and metamorphism (e.g., Gabrielse et al., 1993b; Colpron et al., 2006b; Murphy et al., 2006; Berman et al., 2007). Metamorphism is particularly intriguing because parts of the YTT were metamorphosed to eclogite and blueschist and along the YTT-SMT boundary (Fig. 1) during

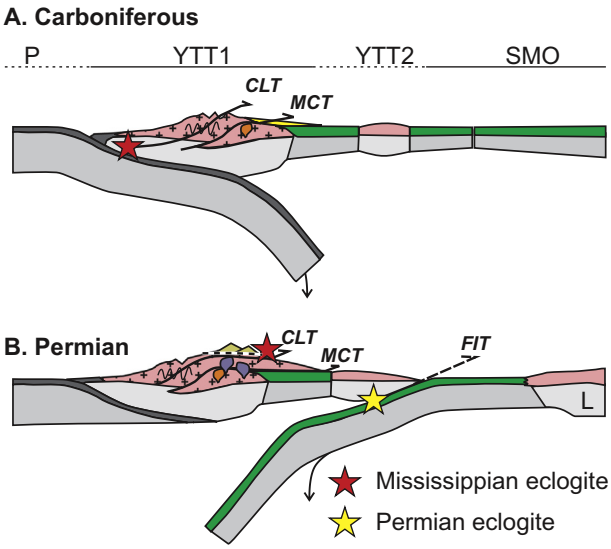

Fig. 2. Schematic late Paleozoic tectonic evolution of the Yukon-Tanana (YTT) and Slide Mountain (SMT) terranes (modified from Devine et al. (2006); Berman et al. (2007)). The principle differences between the Devine et al. (2006) and Berman et al. (2007) models is the degree of fragmentation of YTT and timing of intra-arc shortening. These models imply that SMT ophiolitic rocks form part of the subducting Slide Mountain Ocean (SMO). A. East-directed Late Devonian-Mississippian subduction of Panthalassa Ocean under YTT producing eclogite and arc magmatism (orange plutons). Slab rollback causes arc rifting and opening of the SMO. Early Mississippian intra-arc shortening is generated when westward movement of YTT overtakes slab rollback although backarc opening continues. Dense eclogite produced in the downgoing Panthalassan slab is transferred into the subduction complex and exhumed to shallow levels, the cause of which is unspecified, during continuous eastward-directed subduction and backarc opening. East-directed subduction ceases for unknown reason in the early Permian, causing further intra-arc shortening, followed by a subduction polarity flip into the SMO. B. West-directed subduction of the SMO slab causes the Permian Klondike phase of arc magmatism (purple plutons) in YTT and eclogite facies metamorphism in the east-facing subduction complex. Intra-arc shortening reactivates earlier formed thrusts and transports Mississippian eclogites over the YTT and active? Klondike arc. The final location of the Mississippian eclogites eventually coincides with the YTT-SMT boundary nearly coincident with the location of most Permian eclogites (see Fig. 1). CLT – Cleaver Lake Thrust; FIT – Future Inconnu Thrust; MCT – Money Creek Thrust; L - Laurentia P – Panthalassa Ocean; SMO – Slide Mountain Ocean; YTT1/2 – Yukon Tanana terrane east and west; Devine et al. (2006) suggested that Yukon-Tanana terrane may have been fragmented into several microcontinents.

both the Early Mississippian and Permian (Erdmer and Helmstaedt, 1983; Erdmer et al., 1998; Devine et al., 2006; Petrie et al., 2015; Gilotti et al., 2017; Colpron et al., 2017). Development of high-pressure rocks such as eclogite within the YTT while it occupied an upper plate arc setting can occur when rocks of the arc-trench gap are partially subducted (e.g., Abbott et al., 1994; McIntosh et al., 2005) or dragged down by subduction erosion (Gilotti et al., 2017). The presence of Mississippian eclogite in the upper plate was also explained by east-directed translation of a nappe containing Mississippian eclogite derived from a pre-Permian west-facing forearc/accretionary prism over its associated west-facing arc (Devine et al., 2006). Once the nappe had moved into the retro arc region, it was finally incorporated into an imbricate stack with elements derived from the closing SMO backarc, along the future YTT-SMT boundary (Fig. 2b). However, we are not aware of any recent analogues for such a tectonic scenario, neither do we understand the driving mechanism for such a process.

(iii) Established models infer that the SMO ocean floor, represented by the SMT, was obducted both onto the YTT and Laurentian margin from a lower plate position rather than entering the subduction channel with its parent subducting plate. Normal oceanic crust (formed in a mature backarc or mid-ocean ridge) lacks crustal thickness and buoyancy for collisional orogenesis (e.g., Cloos, 1993) and is almost universally subducted with many of its topographic anomalies, commonly accompanied by subduction erosion of the upper plate (e.g., von Huene and Scholl, 1991; Stern, 2011). Accreting margins only comprise 26% of present day global subduction systems and commonly occur where there is abundant sediment supply to the trench (e.g. Scholl and von Huene, 2007). Some of these accretionary complexes do preserve minor subducting ophiolitic oceanic crust as off-scraped or underplated thrust sheets (e.g., Kimura and Ludden, 1995; Calvert, 1996), but these generally lack mantle sections and are uncommon. Locally, ophiolitic rocks along suture zones do originate from the subducting plate but these are underplated and generally metamorphosed to relatively high grade conditions (e.g., Manatschal et al., 2011; van Staal et al., 2013). Obduction of downgoing plate-derived SMT ophiolitic rocks characterised by low metamorphic-grade, thus does not seem very likely and needs to be re-evaluated along with its relationship to YTT (c.f. Parsons et al., 2018a).

These underlying assumptions and issues relating to SMT-YTT interactions can be tested by establishing constraints on the timing and nature of the mafic-ultramafic complexes along the suture between Slide Mountain and Yukon-Tanana terranes. Consequently, this study is focused on the Clinton Creek and Midnight Dome and ultramafic-mafic complexes west of the Tintina Fault near the town of Dawson (Fig. 1, localities i and k) and a large ultramafic-mafic body of the St. Cyr klippe near Quiet Lake area (Fig. 1, locality d).

3. Existing constraints on the time of opening of the Slide Mountain Ocean

The exact time of SMO opening in the models of Nelson (1993), Nelson et al. (2006) and Colpron et al. (2006a, 2006b, 2007) is difficult to establish with the existing database, because autochthonous Laurentia does not preserve a rift-drift transition of an appropriate age. As such, timing is largely based on circumstantial evidence. Opening is generally inferred to be Famennian-Early Mississipian, largely based on the presence of Famennian-Mississippian rift-related magmatism in both YTT and the Laurentian margin, and an absence of younger magmatism in the Laurentian margin (e.g., Piercey et al., 2003, 2004, 2006). However, the departure of the YTT may have occurred earlier. Late Famennian folding and metamorphism in parts of YTT (e.g. Murphy et al., 2006), but not in the Laurentian margin suggests that YTT was already separated from Laurentia by the late Devonian. This is consistent with the presence of ca. 379 and 364 Ma N-MORB-like intrusive rocks in rocks assigned to the Snowcap assemblage (Petrie et al., 2016), suggesting rifting was in an advanced stage at this time. Similar relationships may be present in the Klatsa metamorphic complex (Fig. 1, Devine et al., 2006), where leucogabbro in Klatsa serpentinite yielded a U-Pb zircon age of ca 368 Ma (Devine et al., 2006). Although the primary relationships are difficult to establish, these Upper Devonian rocks may represent parts of transitional oceanic lithosphere that is overlapped by Upper Devonian Snowcap assemblage sediments throughout the nascent SMO (see Manatschal, 2004; Manatschal et al., 2006). Isolated extensional allochthons of thin continental crust and overlapping continentally-derived sediments could be the source of crustal contamination in Carboniferous-Permian oceanic arc sequences (Parsons et al., 2018a, see below).

4. Constraints on the setting and age of the SMT ophiolitic rocks

Ultramafic-mafic complexes in the SMT were previously mainly interpreted as dismembered ophiolitic slivers that were tectonically

imbricated with the enclosing rocks (e.g. Nelson, 1993; Colpron et al., 2005; Piercey et al., 2012). These ultramafic-mafic complexes are typically dominated by voluminous ultramafic rocks, subordinate gabbroic rocks, and variably abundant mafic volcanic rocks (Nelson, 1993; Colpron et al., 2005; Murphy et al., 2006; Piercey et al., 2012; Ryan et al., 2015; Parsons et al., 2017, 2018a). The ultramafic-mafic complexes in the part of the Finlayson district underlain by YTT rocks (Fig. 1) of southwest Yukon, however, generally were considered to represent layered intrusions (Murphy et al., 2006). In contrast, we interpret the Finlayson district ultramafic-mafic complexes as allochthonous slices of mantle and lower crust. These bodies are locally well exposed in three dimensions, are not obviously layered, but are variably serpentinized, foliated chromite-bearing peridotite, locally preserving a shape fabric defined by chromite and/or bastite pseudomorphs after orthopyroxene. These peridotites are also locally overlain by basalts, which is inconsistent with intrusion in the lower or middle crust. Pegmatitic pyroxenite bodies within the peridotite do not extend into the highly transposed enveloping country rocks and neither do the latter contain mafic-ultramafic feeder dikes and/or satellite sills. In addition, there is no evidence of high temperature contact metamorphism in the country rocks along the base of the thick peridotite bodies (50–500 m). These observations have implications for the tectono-stratigraphy of the YTT, which was established in the Finlayson district in part using these ultramafic rocks as stitching plutons (Murphy et al., 2006) and correlation of distinct basalt-dominated units across faults (cf. Piercey et al., 2012).

Direct age constraints on the ophiolitic ultramafic-mafic complexes in the SMT are sparse (Fig. 1), but come from the Sylvester allochthon in British Columbia (Nelson, 1993; Nelson and Bradford, 1993) and in the Yukon mainly from the Finlayson district (Murphy et al., 2006), the Dunite Peak area (De Keijzer et al., 2000; Parsons et al., 2018a) and the Tummel fault zone and Ragged Lake klippe (Colpron et al., 2005, 2006a, 2006b). Carboniferous or older members of the SMT are preserved in the St. Cyr klippe (see below) and potentially in the Klatsa metamorphic complex in the Finlayson district (Fig. 1), where leucogabbro in serpentinized ultramafic rocks yielded a U-Pb zircon age of 368 ± 10 Ma (Devine et al., 2006). Chert associated with basalt of the Campbell Range Formation, part of the SMT in the Finlayson district, contains mid-Pennsylvanian to Early Permian radiolaria, whereas gabbroic intrusive rocks that cut the basalt yielded ca. 273 Ma U-Pb zircon crystallization ages (Mortensen, 1992; Murphy et al., 2006). The Campbell Range Formation is dominated by enriched and normal mid-ocean ridge (E-MORB, N-MORB and OIB) basalt, but also contains minor greenstone, gabbro and leucogabbro, island arc tholeiitic to calc-alkaline (IAT/CA) basalt and backarc basin basalt (BABB) (Plint and Gordon, 1997; Murphy et al., 2006; Piercey et al., 2006), which have been interpreted to have formed as a result of highly oblique spreading, juxtaposing different backarc settings along giant transform faults in the SMO (Piercey et al., 2012). However these interpretations were in part based on using the ophiolitic ultramafic rocks as stitching intrusions.

The Dunite Peak area preserves structurally dismembered SSZ juvenile ophiolitic rocks with IAT and BABB compositions, structurally emplaced on top of marble and siliciclastic rocks of the Snowcap assemblage (Parsons et al., 2017, 2018a). Associated IAT gabbroic rocks yielded ca. 265 Ma ages (De Keijzer et al., 2000; Parsons et al., 2018a) corresponding to SSZ ophiolite generation in an extensional intra-oceanic arc setting. In the Glenlyon region, mafic rocks with similar IAT to CA geochemical compositions indicative of an SSZ setting were recorded from SMT andesitic greenstones and gabbro in the Tummel fault zone and Ragged Lake klippe, which yielded U-Pb igneous ages of ca. 268 and 260 Ma respectively (Colpron et al., 2005, 2006a, 2006b).

The Sylvester Allochthon in British Columbia (Nelson, 1993; Nelson and Bradford, 1993) preserves several distinct tectono-stratigraphic slices including equivalents of the YTT (Harper Ranch, Division 3 of Nelson, 1993) and SMT (Division 2 of Nelson, 1993). Division 2 SMT comprises basinal sediments and basalt. The basalts are predominantly N-MORB and E-MORB, but a minority have IAT to CA signatures, indicating an SSZ setting (Nelson, 1993). Associated sediments yield Mississippian to middle Permian fossils (Harms and Murchey, 1992; Nelson, 1993). A SMT gabbro-trondhjemite complex at Zus Mountain yielded a ca. 269 Ma U-Pb zircon crystallization age suggesting that the ophiolitic rocks are middle Permian (Gabrielse et al., 1993). Other plutonic rocks in the area, ranging from granite to gabbro, yield similar middle Permian ages (270–262 Ma: Gabrielse et al., 1993; Roback et al., 1994). The existing age data summarized above provide direct constraints on the ophiolitic rocks included in the SMT and YTT in Yukon and British Columbia that suggest an age range from ca. 368 to 260 Ma. Middle Permian ages are typical of the ophiolitic rocks that are exposed near the suture between the oceanic SMT and the Laurentian margin and are broadly coeval with the eclogite facies metamorphism and Klondike orogeny in the YTT. The broadly coeval timing of these events raises the questions as to why the preserved parts of the SMT were formed by spreading in a SSZ setting while the overriding YTT was undergoing collisional orogenesis and eclogite facies metamorphism.

5. Geochronology, geochemistry and setting of the Clinton Creek, Midnight Dome and St. Cyr ultramafic-mafic complexes of the Yukon SMT

5.1. Analytical methods

5.1.1. Zircon U-Pb geochronology

U–Th–Pb isotopic data of zircon crystals from mafic and intermediate igneous rocks closely associated with the ultramafic rocks were analyzed using the sensitive high-resolution ion microprobe-reverse geometry (SHRIMP-RG) mass spectrometer at the U.S. Geological Survey – Stanford Micro-Analysis Center at Stanford University. Zircon grains were separated from 1 to 3 kg samples by standard physical separation techniques and mounted in 2.54 cm epoxy rounds, which were polished to expose grain interiors. Cathodoluminescence (CL), transmitted light, and reflected light images were used to characterize zircon domains, including homogeneous regions of the zircons and to avoid complex internal structures, cracks, and zones of potential Pb loss. Calibration of U was based on zircon standard Madagascar Green (MAD; 4196 ppm U; Barth and Wooden, 2010). Isotopic ratios were calibrated by replicate analyses of zircon standard R33 (421 Ma, Black et al., 2004; Mattinson, 2010), which were rerun after every fourth analysis (Table 1). The analytical routine followed Barth and Wooden (2006, 2010) using a 20 μm spot diameter. Data reduction used Squid 2.51 program of Ludwig (2003). Crystallization ages were calculated as weighted mean 207-corrected $^{206}Pb/^{238}U$ ages and Tera-Wasserburg diagrams were generated using the Isoplot/Ex program of Ludwig (2003). Reported age errors are at the 95% confidence level and incorporate the 2σ external spot-to-spot error of the R33 standard, which was 0.56% and 0.66% for the two mounts analyzed.

Trace-element data for Y, REE, and Hf were collected simultaneously with the U, Th and Pb analyses (Table 1). Data reduction of elemental concentrations used zircon standards MAD (Barth and Wooden, 2010). Chondrite-normalized REE plots (Fig. 3) use the chondrite REE abundances of Anders and Grevesse (1989) multiplied by a factor of 1.36 (Korotev, 1996). Chondrite-normalized values for Pr were calculated by interpolation ($Pr_{(N)} = La_{(N)}^{0.33} \times Nd_{(N)}^{0.67}$). Eu and Ce anomalies are based on $Eu_{(N)}/Eu^*$ and $Ce_{(N)}/Ce^*$ with Eu* and Ce* calculated as geometric means (e.g., $Eu^* = (Sm_{(N)} \times Gd_{(N)})^{0.5}$).

5.1.2. Lithogeochemistry

Whole-rock major and trace element concentrations of the studied mafic and ultramafic rocks were determined by inductively coupled plasma-mass spectrometry (ICP-MS) at Activation Laboratories in Ancaster, Ontario (Table 2). Because rocks in the study area were subjected to greenschist to amphibolite facies metamorphic conditions

Table 1
SIMS Zircon U-Pb geochronologic data, apparent ages and trace element data.

Spot[a]		U (ppm)	Th (ppm)	Th/U	$^{206}Pb^{*}$[b] (ppm)	$f^{206}Pb_c$[b]	$^{238}U/^{206}Pb$[c]	1σ (%)	$^{207}Pb/^{206}Pb$[c]	1σ (%)	$^{206}Pb/^{238}U$[d] (Ma)	1σ	$^{207}Pb/^{206}Pb$[d] (Ma)
VL010-12: Clinton Creek complex, pegmatitic leucogabbro UTMX: 513855; UTMY: 7146707													
11.1	r	2	0.04	0.03	0.03	12.23	45.381	13.8	0.1457	29	123	19	
12.1	r	1	0.01	0.03	0.01	2.72	48.856	19.8	0.0702	48	127	26	
13.1	r	9	1	0.13	0.2	1.93	38.183	9.2	0.06471	27	163	15	
3.1	c	164	122	0.77	5.4	< 0.01	26.214	1.1	0.05099	2.8	241	3	
6.1	r	320	150	0.48	10.8	0.34	25.539	1.2	0.05382	3.0	247	3	
10.1	c	99	42	0.44	3.5	< 0.01	24.623	1.4	0.04897	3.7	**257**	**4**	
8.1	c	127	41	0.33	4.5	0.07	24.153	2.1	0.05204	3.5	**261**	**5**	
14.1	c	133	46	0.36	4.7	< 0.01	24.024	1.2	0.05146	3.1	**263**	**3**	
5.1	c	233	144	0.64	8.4	0.13	23.922	1.0	0.05253	2.3	**264**	**3**	
2.1	c	326	190	0.60	11.8	0.20	23.767	1.0	0.05313	2.6	**265**	**3**	
1,1	c	132	66	0.51	4.8	0.27	23.711	1.2	0.05370	3.0	**266**	**3**	
4.1	c	73	24	0.35	2.7	0.39	23.334	1.5	0.05476	4.1	**269**	**4**	
7.1	c	308	223	0.75	11.3	< 0.01	23.381	1.0	0.05033	2.2	**270**	**3**	
9.1	c	162	107	0.68	6.1	< 0.01	22.724	1.2	0.05129	3.7	278	3	
VL010-09: Midnight Dome complex, leucogabbro UTMX: 578726; UTMY: 7104571													
1.1	c	24	12	0.50	0.8	0.00	26.149	2.6	0.05101	8.3	242	6	
7,1	c	52	30	0.61	1.8	0.60	24.552	1.8	0.05612	5.4	**256**	**5**	
6.1	c	42	20	0.50	1.5	0.96	24.233	1.9	0.05911	5.7	**258**	**5**	
2.1	c	24	12	0.52	0.9	0.62	24.298	2.6	0.05639	7.6	**258**	**7**	
8.1	c	70	40	0.59	2.5	< 0.01	24.234	1.5	0.04657	4.9	**262**	**4**	
5.1	c	28	14	0.52	1.0	< 0.01	23.745	2.3	0.04909	7.5	**267**	**6**	
10.1	c	50	31	0.65	1.8	< 0.01	23.615	1.8	0.05076	5.6	**268**	**5**	
4.1	c	47	28	0.61	1.7	< 0.01	23.507	1.8	0.05062	9.3	**269**	**5**	
3.1	c	16	7	0.45	0.6	0.47	23.170	3.1	0.05545	9.3	**271**	**9**	
9.1	c	49	22	0.45	1.8	0.65	23.101	1.8	0.05690	5.7	**271**	**5**	
VL010-04: St. Cyr klippe, trondhjemite-leucotonalite UTMX: 513855; UTMY: 7146707 615398; UTMY: 6792127													
8.1	m	2515	34	0.014	93.1	0.09	23.219	0.3	0.05244	0.8	272	1	
3.1	m	714	3	0.004	26.6	0.16	23.013	0.4	0.05300	1.2	274	1	
2.1	m	2216	6	0.003	87.6	< 0.01	21.724	0.3	0.05181	0.8	290	1	
6.1	m	1531	14	0.010	61.4	0.30	21.426	0.3	0.05460	1.3	293	1	
12.1	m	1964	7	0.004	79.9	0.03	21.126	0.3	0.05249	1.0	298	1	
4.1	m	2096	8	0.004	87.2	< 0.01	20.650	0.3	0.05194	0.8	**305**	**1**	
10.1	m	657	4	0.006	27.7	0.32	20.365	0.6	0.05511	2.0	**308**	**2**	
14.1	m	1708	7	0.004	72.5	0.04	20.231	0.2	0.05293	0.7	**311**	**1**	
15.1	m	1653	5	0.003	70.4	0.11	20.165	0.3	0.05352	0.8	**312**	**1**	
13.1	m	1201	5	0.004	55.1	0.11	18.721	0.3	0.05404	1.0	335	1	
11.1	r	65	1	0.012	3.1	1.47	17.788	2.6	0.06531	6.9	348	9	1253
7.1	c	197	61	0.32	10.5	0.81	16.033	0.7	0.06094	4.2	387	3	
9.1	c	119	56	0.49	18.7	1.21	5.439	0.8	0.08540	1.3	1076	9	1314
5.1	c	233	123	0.55	65.7	7.71	3.050	0.6	0.17123	0.5	1704	11	2560
1.1	c	158	100	0.66	53.0	6.56	2.559	0.6	0.18091	0.6	2006	13	2656

Spot[a]	1σ	Y (ppm)	La (ppm)	Ce (ppm)	Nd (ppm)	Sm (ppm)	Eu (ppm)	Gd (ppm)	Dy (ppm)	Er (ppm)	Yb (ppm)	Hf (ppm)	Ce/Ce*	Eu/Eu*	Yb/Gd
VL010-12: Clinton Creek complex, pegmatitic leucogabbro UTMX: 513855; UTMY: 7146707															
11.1		207	0.541	1	0.0	0.0	0.02	1	9	63	288	9887	2	0.69	554.4
12.1		2104	0.070	0	0.0	0.1	0.04	2	69	571	2195	8142	1	0.33	1191.9
13.1		6753	0.431	1	0.1	0.4	0.28	22	382	1551	3707	13,245	3	0.29	165.3
3.1		3872	0.188	26	8.8	13.2	9.35	97	353	631	1251	5873	19	0.79	12.8
6.1		1442	1.905	7	0.8	0.8	1.25	22	121	294	679	14,161	2	0.90	30.7

(*continued on next page*)

Table 1 (*continued*)

Spot[a]	1σ	Y (ppm)	La (ppm)	Ce (ppm)	Nd (ppm)	Sm (ppm)	Eu (ppm)	Gd (ppm)	Dy (ppm)	Er (ppm)	Yb (ppm)	Hf (ppm)	Ce/Ce*	Eu/Eu*	Yb/Gd
10.1		1401	0.033	8	1.1	2.4	2.19	22	99	234	549	6767	36	0.93	25.0
8.1		1634	0.125	8	1.0	2.0	1.75	21	115	296	733	7130	16	0.83	35.7
14.1		1241	0.019	4	0.7	2.0	1.88	21	101	223	512	8009	27	0.88	24.2
5.1		3635	0.122	23	5.3	9.2	6.81	78	311	605	1251	6508	26	0.77	16.1
2.1		3780	0.059	20	4.1	8.5	6.44	81	342	649	1336	7236	40	0.75	16.6
1,1		2301	0.124	13	3.3	5.8	4.26	46	199	400	897	7245	17	0.80	19.6
4.1		1553	0.028	7	1.6	2.9	2.28	27	113	277	667	7025	30	0.79	24.7
7.1		4468	0.201	32	9.8	14.9	11.96	118	420	706	1370	9113	21	0.87	11.7
9.1		4500	0.131	27	9.8	15.2	10.74	109	421	761	1572	7000	24	0.80	14.4
VL010-09: Midnight Dome complex, leucogabbro UTMX: 578726; UTMY: 7104571															
1.1		2200	0.012	6	1.7	4.9	1.88	53	211	389	648	7922	42	0.35	12.1
7,1		3350	0.040	10	2.4	7.2	3.02	82	342	599	991	8073	31	0.38	12.1
6.1		2673	0.025	9	2.2	5.9	1.75	63	242	453	762	9211	37	0.28	12.1
2.1		324	0.026	2	0.2	0.6	0.39	7	33	57	98	9277	14	0.57	13.7
8.1		2320	0.031	6	2.4	6.7	1.97	63	232	387	603	7646	24	0.29	9.5
5.1		2084	0.023	5	1.6	4.5	1.52	48	192	358	620	8318	26	0.31	12.9
10.1		4475	0.023	15	4.0	12.2	3.55	118	447	775	1224	8243	57	0.28	10.3
4.1		1335	0.043	3	1.1	2.3	0.91	21	103	252	467	8777	10	0.39	21.8
3.1		1419	0.026	4	1.2	3.5	1.11	35	134	246	418	8075	23	0.31	12.1
9.1		2483	0.024	11	0.7	2.4	1.07	33	203	460	846	8410	69	0.37	26.0
VL010-04: St. Cyr klippe, trondhjemite-leucotonalite UTMX: 513855; UTMY: 7146707 615398; UTMY: 6792127															
8.1		145	1.419	6	3.4	3.1	1.26	10	23	18	18	12,270	2	0.68	1.8
3.1		184	1.082	2	0.2	0.2	0.12	2	13	33	65	5666	2	0.51	28.7
2.1		321	0.025	0	0.1	0.3	0.26	5	30	70	201	11,977	5	0.65	42.8
6.1		496	0.167	1	0.7	0.8	0.30	5	39	114	339	11,735	2	0.45	62.1
12.1		327	1.505	4	0.8	0.6	0.27	4	25	65	206	9896	1	0.50	47.4
4.1		367	0.662	1	0.4	0.5	0.30	5	31	77	215	11,068	1	0.59	41.4
10.1		123	3.193	6	0.6	0.5	0.23	3	10	18	39	4686	2	0.56	12.1
14.1		452	0.072	1	0.3	0.4	0.19	5	40	83	144	11,526	2	0.39	30.7
15.1		695	0.017	0	0.0	0.3	0.11	5	55	146	341	12,106	6	0.28	68.7
13.1		621	0.053	0	0.1	0.3	0.11	4	49	131	307	11,273	3	0.30	71.3
11.1	241	58	1.179	2	0.2	0.2	0.04	1	4	8	16	6318	2	0.35	24.9
7.1		710	0.190	4	1.3	2.3	0.26	19	70	123	205	9655	5	0.12	11.0
9.1	26	984	0.116	12	4.1	5.9	0.69	38	121	173	273	8089	15	0.14	7.2
5.1	9	552	1.129	16	5.9	6.1	2.06	23	71	99	170	9137	4	0.52	7.3
1.1	10	300	0.124	39	1.2	2.2	0.84	12	30	49	100	8213	70	0.49	8.3

Note: All analyses were performed on the SHRIMP-RG ion microprobe at the United States Geological Survey-Stanford Microanalytical Center at Stanford University. The analytical routine followed Barth and Wooden (2006, 2010).

Data reduction utilized the Squid 2.51 program of Ludwig (2003).

Ages in bold were used in age calculation.

[a] Abbreviations and CL designations: c = core; m = CL-dark mantle; r = rim.

[b] Pb* denotes radiogenic Pb; Pbc denotes common Pb; $f^{206}Pbc = 100 * (^{206}Pbc/^{206}Pbtotal)$.

[c] Calibration concentrations and isotopic compositions were based on replicate analyses of R33 (421 Ma, Black et al., 2004; Mattinson, 2010) and Madagascar Green (MADDER; 3435 ppm U, Barth and Wooden, 2010). Reported ratios are not corrected for common Pb. Errors are reported in parentheses as percent at the 1σ level.

[d] Ages were calculated from $^{206}Pb/^{238}U$ ratios corrected for common Pb using the ^{207}Pb method (see Williams, 1998). Initial common Pb isotopic composition approximated from Stacey and Kramers (1975). Uncertainties in millions of years reported as 1σ.

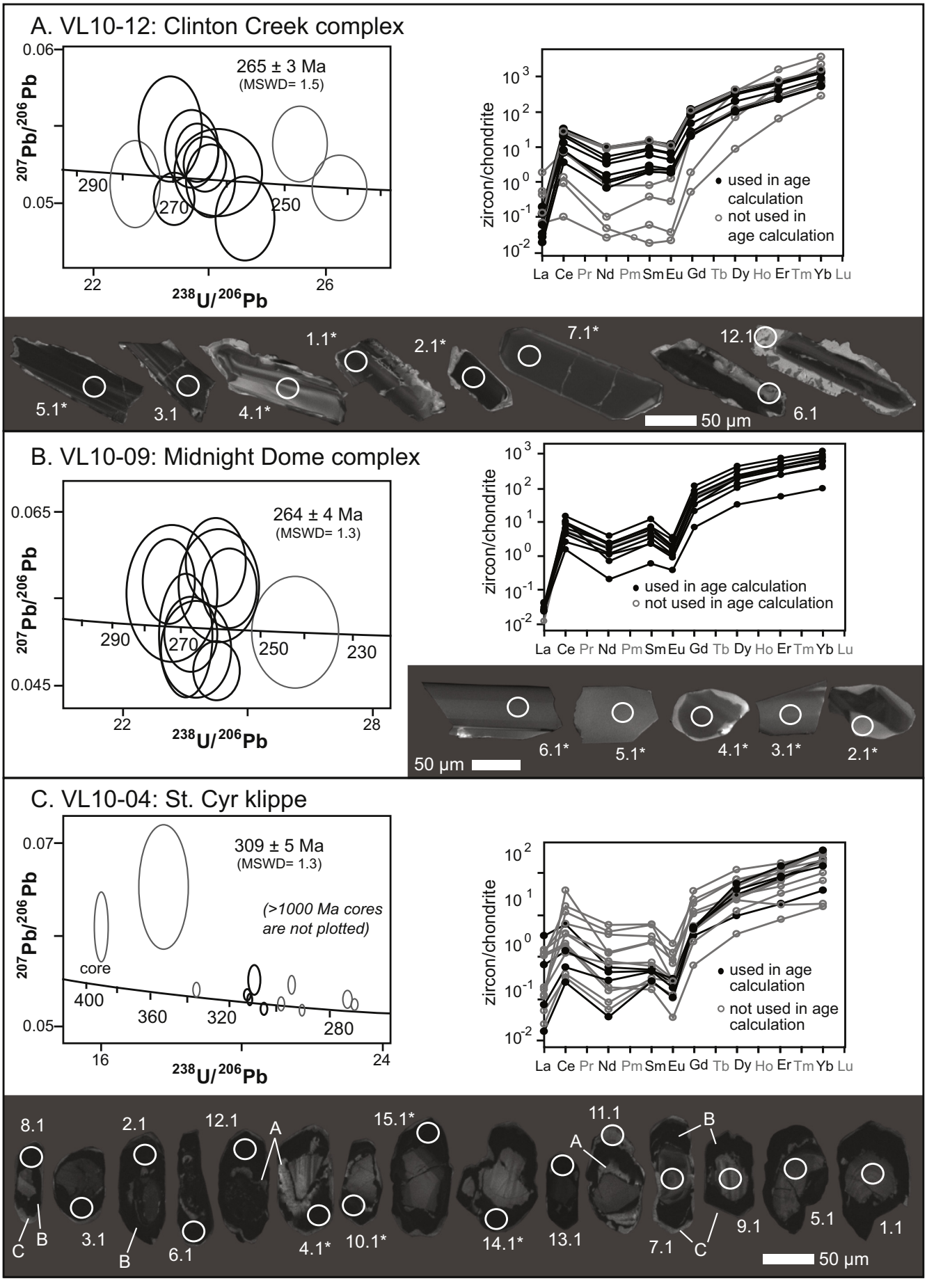

(caption on next page)

Fig. 3. Tera-Wasserburg plots, chondrite-normalized rare earth plots, and cathodoluminescence images of zircon from the Clinton Creek (VL10-12), Midnight Dome (VL10-09) and St. Cyr (VL10-04) complexes. U/Pb data plotted as 1σ error ellipses uncorrected for common Pb. Black ellipses and grains noted with * in CL images are used in calculating weighted mean ages. Weighted mean age uncertainty is reported at the 95% confidence level. Letters in 3c show inner rims (A), CL-dark mantles that are interpreted to represent zircon growth during trondhjemite-leucotonalite crystallization (B) and outermost rims (C).

and major and low field strength elements are likely to have been mobile (e.g., Na, K, Ca, Si, Cs, Ba, Rb). As such, geochemical discriminations utilized herein are based mainly on high field-strength elements (HFSE: Hf, Nb, Ta, Ti, Sc, Y, Zr), rare earth elements (REE), and Th which are considered to be immobile under typical greenschist to amphibolite facies conditions (e.g., Pearce, 1996).

5.1.3. Microprobe

Electron microprobe analyses of chromian spinel were carried out on polished sections of serpentinites. Analyses were conducted with a four-channel CAMECA SX50 electron microprobe at the Serveis Cientificotècnics of the Universitat de Barcelona (Barcelona, Spain). Mineral compositions were obtained by analyzing several grains in each section (Table 3). The analytical conditions were 20 kV accelerating voltage, 20 nA beam current, 2 μm beam diameter, and counting time of 10 s per element. Calibrations were performed using natural and synthetic reference materials: chromite (Cr, Al, Fe), periclase (Mg), rhodonite (Mn), rutile (Ti), NiO (Ni) and metallic V. The proportion of trivalent iron in chromian spinel was calculated assuming stoichiometry.

5.2. Clinton Creek complex

The Clinton Creek complex (Abbott, 1983) occurs close to the Alaska-Yukon border (Fig. 1) and was previously correlated with ultramafic-mafic rocks of the Seventymile terrane, a correlative of the SMT in Alaska, which are associated with Permian and Triassic volcanic and sedimentary rocks (Foster and Keith, 1974; Foster et al., 1994; Dusel-Bacon et al., 2006 and references therein). The Clinton Creek complex mainly comprises a sheared assemblage of strongly altered ultramafic rocks with minor mafic intrusive rocks and is associated with greenschist facies tectonites of uncertain origin (Abbott, 1983). These rocks occur as generally shallowly dipping, sheared lenses within weakly metamorphosed sedimentary rocks. Sedimentary rocks yielded one conodont suggestive of a Norian age (Orchard, 2006). The ultramafic rocks were subjected to pervasive low-grade metamorphism and/or hydrothermal alteration, which produced abundant serpentinite and listwaenite (Fig. 4a) and destroyed most primary features. K-Ar and Rb-Sr age determinations of the intimately associated mafic rocks and schist yielded Permian ages (Htoon, 1981). The serpentinite is intruded by leucogabbro (diorite of Abbott, 1983), which locally has coarse pegmatitic patches (Fig. 4b) which were sampled for geochronology.

5.2.1. Geochronology

The sampled pegmatitic leucogabbro gabbro (VL10-12) cuts serpentinized and altered ultramafic rocks, but is itself also cut by fractures, carbonate veins and is locally altered to chlorite, serpentinite and carbonate-bearing assemblages (Fig. 4b). Plagioclase is saussuritizised. The gabbro thus postdates at least some of the alteration and serpentinization of the ultramafic rocks, but is itself also affected by it, suggesting the gabbro intruded while hydrothermal alteration was active in the host. The sample yielded a small population of elongate subhedral zircon with oscillatory zoned to unzoned cores overgrown by unzoned, CL-bright, 2- to 25-μm-thick rims (Fig. 3a). Core analyses lack a well-developed Eu anomaly (Eu/Eu* = 0.8–0.9) but have steep HREE patterns (Yb/Gd = 12–36). The rim analyses show steeper HREE patterns (Yb/Gd = 165–1192) and lower middle REE concentrations, demonstrating that they are chemically distinct from the core domain (Fig. 3a). Eight of nine core analyses give a $^{206}Pb/^{238}U$ age of 265 ± 3 Ma (MSWD = 1.5; Fig. 3). This age is interpreted as the crystallization age of the leucogabbro and the age of mafic magmatism in the Clinton Creek complex. This age is also interpreted to provide a minimum age constraint on the exhumation and serpentinization of the host harzburgite. The latter indicated by gabbro intrusion during high-level hydrothermal alteration of the ultramafic host rocks. The two youngest rim analyses suggest the timing of rim growth is ca 125 Ma.

5.2.2. Geochemical characteristics

The dated leucogabbro is characterised by a flat profile with strong Nb depletion on a N-MORB normalized trace element plot (Fig. 5a), characteristic of arc-related tholeiitic magmas. The sample plots in the volcanic arc tholeiite field (VAT) on tectonic discrimination diagrams (e.g. Fig. 5b). Positive Eu anomaly suggests plagioclase accumulation and is consistent with gabbroic nature of the host and pegmatitic nature of the sample. Altered ultramafic rocks yield harzburgite (Al_2O_3 0.28 wt %) and websterite (Al_2O_3 1.78 wt%) normative compositions (Fig. 5d), consistent with poorly preserved serpentine pseudomorphs after olivine and orthopyroxene. Trace element concentrations in harzburgite are near or below the analytical detection limit; however, the sample shows slight LREE enrichment relative to HREE (Gd and Dy) on a primitive mantle-normalized plot (Fig. 5c). Websterite shows a consistent negative slope on a primitive mantle normalized diagram and a flat slope on N-MORB normalized diagram (Fig. 5a, c).

5.3. Midnight Dome complex

The Midnight Dome ultramafic-mafic complex (Mortensen, 1990) occurs near the town of Dawson City (Fig. 1) roughly on strike with the Clinton Creek complex, which it closely resembles lithologically and in style of deformation and alteration. As in Clinton Creek, an intrusive leucogabbro (Fig. 4c) dike in the ultramafic rocks was sampled for geochronology.

5.3.1. Geochronology

The sampled leucogabbro (VL10-09) has coarse pegmatitic pods and is locally weakly foliated (Fig. 4c). The leucogabbro cuts the altered and serpentinized peridotite, but itself generally displays good preservation of primary textures and little alteration (Fig. 4c). The sample yielded a small population of elongate crystals that display coarse oscillatory zoning in CL images (Fig. 3b). Zircons display well developed Eu anomalies (Eu/Eu* = 0.3–0.6) and steep HREE patterns (Yb/Gd = 10–26; (Fig. 3b). U/Pb analyses range from 241 to 268 Ma. Assuming the youngest analysis reflects Pb-loss, nine of ten analyses define a $^{206}Pb/^{238}U$ weighted mean age of 264 ± 4 Ma (MSWD = 1.3; Fig. 3b). This age is interpreted as the crystallization age of the gabbro and the age of mafic magmatism in the Midnight Dome complex. This age is also interpreted to provide a minimum time constraint on the exhumation and alteration of the host harzburgite.

5.3.2. Geochemical characteristics

Dated leucogabbro is characterised by a flat N-MORB normalized trace element profile with strong positive Eu anomaly indicative of plagioclase accumulation (Fig. 5a). Th and Nb are below the detection limit. Other mafic samples (2 gabbro and 1 diabase) from the same complex have similarly flat REE profiles on an N-MORB normalized diagram. Gabbro and diabase have strong Nb depletion characteristic of arc-related tholeiitic magmas (Fig. 5a). These two samples plot in the volcanic arc tholeiite field (VAT) on tectonic discrimination diagrams (e.g. Fig. 5b). Altered ultramafic rocks yield harzburgite normative compositions (Fig. 5d), consistent with poorly preserved textural

Table 2
Whole rock geochemical data (major elements at wt% oxides, trace and rare earth elements in ppm) for the St. Cyr, Clinton Creek (CC) and Midnight Dome (MD) complexes. See text for methods used. B.D. = below detection.

Sample	VL10-02	VL10-07	VL10-08	VL10-10	VL10-11	VL10-12	VL10-09	10VLE-A101-02	10VLE-A101-03	10VLE-A101-04	10VLE-A101-05	10VLE-A101-06	10VLE-A101-07	10VLE-A101-08	10VLE-A101-09	10VLE-A101-10	10VLE-A101-12	10VLE-A101-13
Complex	St. Cyr	St. Cyr	St. Cyr	CC	CC	CC	MD	MD	MD	MD	MD	MD	MD	MD	MD	MD	MD	MD
Lithology	peridotite	peridotite	peridotite	peridotite	websterite/gabbro	gabbro	gabbro	peridotite	peridotite	peridotite	peridotite	peridotite	peridotite	gabbro	gabbro	peridotite	peridotite	diabase
UTMX	629509	615202	603281	513855	513855	514067	578811	578726	578726	578726	578726	578726	578726	578726	578726	578726	578726	578726
UTMY	6785757	6791831	6799407	7146707	7146707	7146561	7704372	7104571	7104571	7104571	7104571	7104571	7104571	7104571	7104571	7104571	7104571	7104571
SiO_2	41.23	39.66	35.98	38.7	55.19	40.95	50.3	39.41	41.94	39.78	40.4	39.8	40.91	51.86	47.84	40.72	40.42	53.16
Al_2O_3	1.13	0.53	0.74	0.28	1.76	16.47	16.53	0.83	0.46	0.49	0.71	0.98	0.71	15.03	16.34	0.73	0.55	16.06
Fe_2O_3	8.7	7.8	14	5.26	4.75	11.01	6.98	10.03	7.32	8.56	7.75	7.98	7.56	9.26	10.66	7.65	9.76	9.52
MnO	0.13	0.056	0.116	0.095	0.089	0.16	0.138	0.058	0.088	0.077	0.072	0.069	0.074	0.185	0.159	0.075	0.056	0.137
MgO	41.26	39.63	35.75	39.07	19.57	9.11	8.6	36.86	38.74	37.1	39.1	38.23	39.4	6.04	6.16	38.47	37.99	6.15
CaO	1.15	0.02	0.27	1	16.37	14.86	7.99	0.14	0.1	0.04	0.03	0.02	0.02	9.81	9.82	0.04	0.02	5.53
Na_2O	0.02	B.D.	0.01	0.02	0.16	0.45	2.7	0.01	0.01	B.D.	B.D.	B.D.	0.01	3.38	3.33	0.01	0.01	3.93
K_2O	B.D.	B.D.	B.D.	B.D.	0.03	0.48	1.92	0.01	0.01	0.01	B.D.	B.D.	B.D.	0.2	0.06	B.D.	B.D.	0.02
TiO_2	0.053	0.007	0.01	0.005	0.121	1.405	0.275	0.009	0.005	0.004	0.01	0.013	0.009	1.185	1.344	0.012	0.011	0.482
P_2O_5	B.D.	0.03	B.D.	0.02	0.03	0.13	B.D.	0.03	B.D.	B.D.	0.04	B.D.	B.D.	0.14	0.08	B.D.	B.D.	0.06
LOI	6.43	12.47	12.01	15.9	2.74	4.79	3.88	12.17	12.09	11.96	11.84	11.79	11.87	3.07	4.71	11.64	11.58	3.58
Total	100.1	100.2	98.91	100.4	100.8	99.81	99.32	99.57	100.8	98.04	99.96	98.9	100.6	100.2	100.5	99.36	100.4	98.64
Ba	B.D.	9	B.D.	536	33	3282	1519	11	13	15	23	18	28	80	80	4	11	12
Co	115	95	94	79	50	40	27	91	83	90	78	68	71	27	30	84	96	27
Cr	2470	2770	2600	2420	1770	200	250	2550	2530	3150	2520	2570	2400	120	130	2700	2530	20
Cs	B.D.	B.D.	B.D.	1.4	7.4	2.5	1.1	0.2	0.3	0.1	B.D.	B.D.	B.D.	0.1	0.4	B.D.	B.D.	B.D.
Cu	10.3	2.1	17.3	2.8	2.7	8.8	1.6	15.3	27.9	6.7	9.5	8.3	8.8	64.8	96.4	12.5	9.1	81.7
Hf	B.D.	B.D.	B.D.	B.D.	0.2	2.2	0.3	B.D.	B.D.	B.D.	B.D.	B.D.	B.D.	1.7	1.9	B.D.	B.D.	0.6
Nb	B.D.	B.D.	B.D.	B.D.	B.D.	0.6	B.D.	B.D.	B.D.	B.D.	B.D.	B.D.	B.D.	0.7	1	B.D.	B.D.	B.D.
Ni	2100	2190	2060	2120	451	87	133	1990	2040	2650	1890	1560	1520	60	69	2270	2300	49
Pb	B.D.	B.D.	B.D.	B.D.	B.D.	B.D.	B.D.	2	B.D.	B.D.	B.D.	B.D.	B.D.	B.D.	B.D.	B.D.	B.D.	B.D.
Rb	B.D.	B.D.	B.D.	B.D.	2	12	22	B.D.	B.D.	B.D.	B.D.	B.D.	B.D.	6	B.D.	B.D.	B.D.	B.D.
Sr	B.D.	B.D.	B.D.	85	36	357	92	5	2	B.D.	B.D.	B.D.	B.D.	117	90	B.D.	B.D.	97
Ta	B.D.	B.D.	B.D.	B.D.	B.D.	0.06	B.D.	B.D.	B.D.	B.D.	B.D.	B.D.	B.D.	0.04	0.08	B.D.	B.D.	0.02
Th	B.D.	B.D.	B.D.	B.D.	B.D.	0.1	B.D.	0.13	0.05	B.D.	B.D.	B.D.	B.D.	0.15	0.17	B.D.	B.D.	0.12
U	B.D.	0.02	B.D.	B.D.	0.28	0.07	0.02	0.23	0.15	0.15	0.02	0.03	0.02	0.12	0.08	0.01	0.02	0.14
V	42	30	42	20	67	308	148	29	27	22	26	28	27	350	389	31	31	294
Y	1.3	B.D.	1.1	B.D.	2.7	31	6.5	1.2	B.D.	B.D.	0.8	1.2	0.7	25.2	27.5	0.8	0.7	12.2
Zr	2	B.D.	B.D.	B.D.	5	83	10	B.D.	B.D.	B.D.	B.D.	B.D.	B.D.	66	72	B.D.	B.D.	22
La	0.38	0.22	0.25	0.13	0.27	3.48	0.68	2.39	0.48	0.45	0.61	0.33	0.64	3.5	3.55	0.19	0.3	1.24
Ce	0.62	0.53	0.25	0.25	0.81	10.6	1.84	3.67	0.53	0.52	1.01	0.66	0.87	9.66	10.2	0.4	0.49	3.05
Pr	0.08	0.06	0.07	0.03	0.14	1.85	0.32	0.37	0.1	0.08	0.11	0.07	0.07	1.59	1.68	0.05	0.07	0.5
Nd	0.41	0.2	0.23	0.11	0.81	10.2	1.6	1.26	0.38	0.32	0.47	0.36	0.32	8.26	8.61	0.26	0.34	2.61
Sm	0.1	0.03	0.07	0.03	0.27	3.52	0.58	0.17	0.05	0.04	0.07	0.13	0.1	2.84	2.86	0.04	0.08	0.93
Eu	0.035	0.016	0.01	0.008	0.088	1.77	0.402	0.041	0.028	0.032	0.021	0.015	0.019	1.04	1.09	0.015	0.022	0.405
Gd	0.18	0.03	0.16	0.03	0.41	4.93	1.02	0.18	0.07	0.07	0.12	0.17	0.12	3.78	4.15	0.11	0.08	1.52
Tb	0.04	B.D.	0.03	B.D.	0.08	0.87	0.17	0.03	0.01	0.01	0.02	0.03	0.02	0.72	0.77	0.02	0.02	0.32
Dy	0.23	0.03	0.21	0.03	0.55	5.76	1.2	0.19	0.08	0.09	0.14	0.19	0.14	4.49	4.81	0.15	0.12	2.05
Ho	0.05	B.D.	0.03	B.D.	0.1	1.18	0.24	0.04	0.02	0.02	0.03	0.04	0.03	0.93	1.05	0.03	0.02	0.47
Er	0.15	0.01	0.09	B.D.	0.3	3.56	0.74	0.1	0.04	0.05	0.09	0.14	0.08	2.73	3.09	0.1	0.08	1.44
Tm	0.027	B.D.	0.018	B.D.	0.052	0.525	0.112	0.017	0.005	0.01	0.014	0.024	0.015	0.396	0.464	0.017	0.016	0.229
Yb	0.17	0.02	0.14	B.D.	0.32	3.45	0.79	0.14	0.04	0.07	0.09	0.15	0.09	2.64	3.11	0.1	0.11	1.54
Lu	0.025	0.004	0.022	B.D.	0.059	0.562	0.128	0.027	0.005	0.009	0.016	0.021	0.011	0.42	0.481	0.015	0.014	0.258

Table 3
- Microprobe analyses of chromian spinel in peridotite of Midnight Dome complex.

Sample	10VLE-101-05												
UTMX	582490												
UTMY	7105755												
Crystal	sp1-1	sp1-2	sp1-3	sp1-4	sp1-5	sp1-6	sp2-1	sp2-2	sp2-3	sp2-4	sp2-5	sp2-6	sp3-1
SiO_2	0.09	0.12	0.08	0.12	0.04	0.05	0.09	0.09	0.12	0.49	0.05	0.09	0.1
TiO_2	0.07	0.03	0.06	0.09	0.05	0.08	0.05	0.06	0.05	0.08	0.08	0.07	0.06
Al_2O_3	21.02	20.91	20.96	20.62	20.98	20.47	19.87	20.22	20.35	20.35	20.47	20.21	20.99
Cr_2O_3	47.81	47.84	48.54	48.59	48.25	48.89	48.8	49.17	49.13	48.49	48.89	49.06	48.12
Fe_2O_3	1.94	1.73	1.99	2.07	1.79	2.08	2.1	1.92	1.88	1.26	2.08	1.79	1.97
FeO	15.12	15.01	15.43	15.15	15.31	15.69	15.32	15.68	15.42	16.28	15.69	15.88	15.5
V_2O_3	0.22	0.18	0.21	0.19	0.22	0.18	0.21	0.19	0.15	0.23	0.18	0.13	0.33
MnO	0.28	0.25	0.19	0.3	0.29	0.19	0.22	0.2	0.29	0.28	0.31	0.18	0.4
MgO	13.02	12.99	12.77	12.97	13.14	12.95	12.77	12.73	12.86	12.67	12.72	12.59	12.9
ZnO	0.15	0.17	0.26	0.2	0.1	0.1	0.15	0.19	0.26	0.12	0.16	0.16	0.07
Total	99.73	99.24	100.26	100.75	100.35	99.87	99.57	100.45	100.51	100.25	100.63	100.17	100.43
Chromite composition													
Si	0.003	0.004	0.002	0.003	0.004	0.001	0.003	0.003	0.004	0.015	0.001	0.003	0.003
Ti	0.002	0.001	0.002	0.001	0.002	0.001	0.001	0.001	0.001	0.002	0.002	0.002	0.001
Al	0.768	0.768	0.766	0.76	0.75	0.766	0.732	0.738	0.742	0.743	0.746	0.74	0.763
Cr	1.172	1.178	1.175	1.181	1.186	1.182	1.206	1.204	1.201	1.188	1.195	1.205	1.174
Fe^{3+}	0.045	0.041	0.045	0.046	0.048	0.042	0.049	0.045	0.044	0.029	0.048	0.042	0.046
Fe^{2+}	0.392	0.391	0.404	0.397	0.391	0.397	0.4	0.406	0.399	0.422	0.406	0.413	0.4
V	0.006	0.005	0.007	0.005	0.005	0.005	0.005	0.005	0.004	0.006	0.005	0.003	0.008
Mn	0.007	0.007	0.005	0.008	0.007	0.005	0.006	0.005	0.008	0.007	0.008	0.005	0.01
Mg	0.602	0.603	0.589	0.595	0.605	0.598	0.595	0.588	0.593	0.585	0.586	0.583	0.593
Zn	0.003	0.004	0.006	0.005	0.002	0.002	0.003	0.004	0.006	0.003	0.004	0.004	0.001

Sample	10VLE-101-05		10VLE-101-10												
UTMX	582490		578294												
UTMY	7105755		7105301												
Crystal	sp3-2	sp3-3	sp1-1	sp1-2	sp1-3	sp1-4	sp1-5	sp1-6	sp2-1	sp2-2	sp2-3	sp2-4	sp2-5	sp2-6	sp2-7
SiO_2	0.08	0.04	0.11	0.09	0.08	0.06	0.11	0.08	0.06	0.07	0.15	0.08	0.04	0.11	0.08
TiO_2	0.05	0.08	0.06	0.04	0.02	0.07	0.05	0.08	0.04	0.02	0.04	0.09	0.04	0.05	0.06
Al_2O_3	21.09	21.02	18.93	19.03	18.88	19.19	19.21	19.02	18.41	18.24	18.54	18.26	18.3	18.46	18.51
Cr_2O_3	48.33	48.48	47.73	47.26	47.52	47.21	47.28	47.11	49.29	49.28	49.27	48.89	48.8	49.45	49.27
Fe_2O_3	1.94	1.96	4.53	4.48	4.64	4.32	4.17	4.35	3.08	3.39	3.24	3.54	3.51	3.09	3.52
FeO	15.79	15.82	17.13	17.76	17.57	17.22	17.29	17.6	16.7	16.52	16.51	16.46	16.6	16.57	16.74
V_2O_3	0.25	0.2	0.3	0.27	0.27	0.32	0.28	0.26	0.24	0.37	0.23	0.25	0.29	0.23	0.25
MnO	0.24	0.25	0.26	0.26	0.25	0.26	0.33	0.22	0.28	0.23	0.27	0.17	0.28	0.25	0.3
MgO	12.82	12.73	11.73	11.24	11.36	11.54	11.5	11.25	11.69	11.92	12	11.94	11.7	11.95	11.87
ZnO	0.11	0.2	0.19	0.15	0.16	0.2	0.15	0.25	0.2	0.07	0.2	0.15	0.14	0.14	0.16
Total	100.69	100.78	100.96	100.59	100.74	100.38	100.37	100.21	99.99	100.11	100.45	99.82	99.7	100.31	100.75
Chromite composition															
Si	0.002	0.001	0.003	0.003	0.002	0.002	0.003	0.003	0.002	0.002	0.005	0.003	0.001	0.004	0.003
Ti	0.001	0.002	0.002	0.001	0.001	0.002	0.001	0.002	0.001	0.001	0.001	0.002	0.001	0.001	0.001
Al	0.765	0.763	0.697	0.705	0.698	0.71	0.711	0.707	0.685	0.677	0.685	0.68	0.683	0.683	0.683

(*continued on next page*)

Table 3 (*continued*)

Sample	10VLE-101-05		10VLE-101-10										
UTMX	582490		578294										
UTMY	7105755		7105301										
Crystal	sp3-2	sp3-3	sp1-1	sp1-2	sp1-3	sp1-4	sp1-5	sp1-6	sp2-1	sp2-2	sp2-3	sp2-4	sp2-5	sp2-6	sp2-7
Cr	1.176	1.181	1.179	1.174	1.179	1.172	1.174	1.175	1.23	1.228	1.221	1.221	1.221	1.228	1.22
Fe^{3+}	0.045	0.045	0.106	0.106	0.11	0.102	0.098	0.103	0.073	0.08	0.077	0.084	0.084	0.073	0.083
Fe^{2+}	0.406	0.408	0.448	0.467	0.461	0.452	0.454	0.464	0.441	0.435	0.433	0.435	0.439	0.435	0.438
V	0.006	0.005	0.008	0.007	0.007	0.008	0.007	0.006	0.006	0.009	0.006	0.006	0.007	0.006	0.006
Mn	0.006	0.006	0.007	0.007	0.007	0.007	0.009	0.006	0.007	0.006	0.007	0.004	0.008	0.007	0.008
Mg	0.588	0.584	0.546	0.527	0.531	0.54	0.538	0.529	0.55	0.56	0.561	0.562	0.552	0.559	0.554
Zn	0.003	0.005	0.004	0.004	0.004	0.005	0.003	0.006	0.005	0.002	0.005	0.004	0.003	0.003	0.004

characteristics, as in the Clinton Creek complex. On primitive-mantle normalized trace element diagrams (Fig. 5c), these samples show prominent LREE enrichment and Ti depletion. On major element diagrams (not shown), these samples plot in depleted harzburgite fields (Al_2O_3 0.46 to 0.98). Harzburgite contains unaltered Cr-spinel crystals, which were analyzed using a scanning electron microprobe. Cr- spinel is compositionally homogeneous with high Cr# and Mg#, and very low TiO_2 concentration (Table 3). These analyses plot in the SSZ forearc peridotite fields on spinel tectonic discrimination diagrams (Fig. 6).

5.3.3. St. Cyr klippe ultramafic-mafic rocks

The St. Cyr klippe lies northeast of Quiet Lake (Fig. 1) and contains several structural slices including ultramafic and mafic rocks and YTT Snowcap assemblage rocks (Fallas et al., 1998; Petrie et al., 2015; Gilotti et al., 2017). MORB or BABB-like amphibolite correlated with the SMT is intruded by a hornblende tonalite which yielded a 373 ± 1 Ma U-Pb zircon age (Fallas et al., 1998). The presence of several structural slices displaying a wide range of metamorphic grade within the St. Cyr klippe (Petrie et al., 2015; Gilotti et al., 2017) and the presumed tectonic contact with the ultramafic rocks leaves the age of the ultramafic and entrained mafic rocks poorly constrained. We sampled an intrusive trondhjemite to leucotonalite body (VL10-04) that cuts both the chromite bearing serpentinized ultramafic rocks and small entrained pyroxenite and gabbro intrusive bodies (Fig. 4d) for geochronology. Chromite in the serpentinite locally preserves a shape fabric parallel to the foliation (Fig. 4e).

5.3.4. Geochronology

The sample (VL10-04) yielded a population of subhedral zircon with complex internal zoning. Most grains contain oscillatory zoned cores that are overgrown by at least three rim domains. A discontinuous, 1- to 10-μm-thick, CL-light inner rim typically truncates zoning in the cores (A in Fig. 3c). The inner rim is overgrown by a 5- to 50-μm-thick, CL-dark mantle that is in turn overgrown by a 1- to 20-μm-thick, CL-light outer rim (B and C in Fig. 3c, respectively). The cores give ages between 387 ± 3 Ma and 2656 ± 10 Ma with Th/U ratios of 0.3–0.7 that are characteristic of magmatic zircon. The CL-dark mantle domain, which appears to reflect the bulk of new zircon growth, yielded $^{206}Pb/^{238}U$ ages of between 335 ± 1 Ma and 272 ± 1 Ma with Th/U ratios of 0.003–0.014. A single spot in the outermost low U (65 ppm) rim domain gave an age of 348 ± 9 Ma but the age is compromised by relatively high common Pb and large uncertainty. The mantle domain is inferred to represent zircon growth at the time of trondhjemite-leucotonalite crystallization. The older (> 300 Ma) CL-dark mantle analyses likely reflect mixtures of core and rim domains and younger CL-dark (> 275 Ma) rim analyses likely reflect Pb-loss and/or metamorphism. The remaining subset of CL-dark mantle analyses defines a $^{206}Pb/^{238}U$ age of 309 ± 5 Ma (n = 4/11, MSWD = 1.3) that is interpreted as the best approximation for the trondhjemite-leucotonalite crystallization age (Fig. 3c) and provides a minimum age of the pyroxenite and gabbroic magmatism associated with the ultramafic rocks.

5.3.5. Geochemical characteristics

The serpentinized ultramafic rocks show no obvious compositional layering and are chromite-bearing peridotites with harzburgite normative compositions (Fig. 5d). On primitive-mantle normalized trace element diagrams (Fig. 5c), these samples show prominent Ti depletion, LREE enrichment and slight U-shaped trace element and rare earth patterns.

6. Discussion

The Midnight Dome and Clinton Creek complexes are dominated by highly altered and serpentinized, depleted harzburgite intruded by small bodies of leucogabbro and rare diabase. Complete Penrose-type ophiolitic crustal sections characterised by a pseudo-stratigraphy of

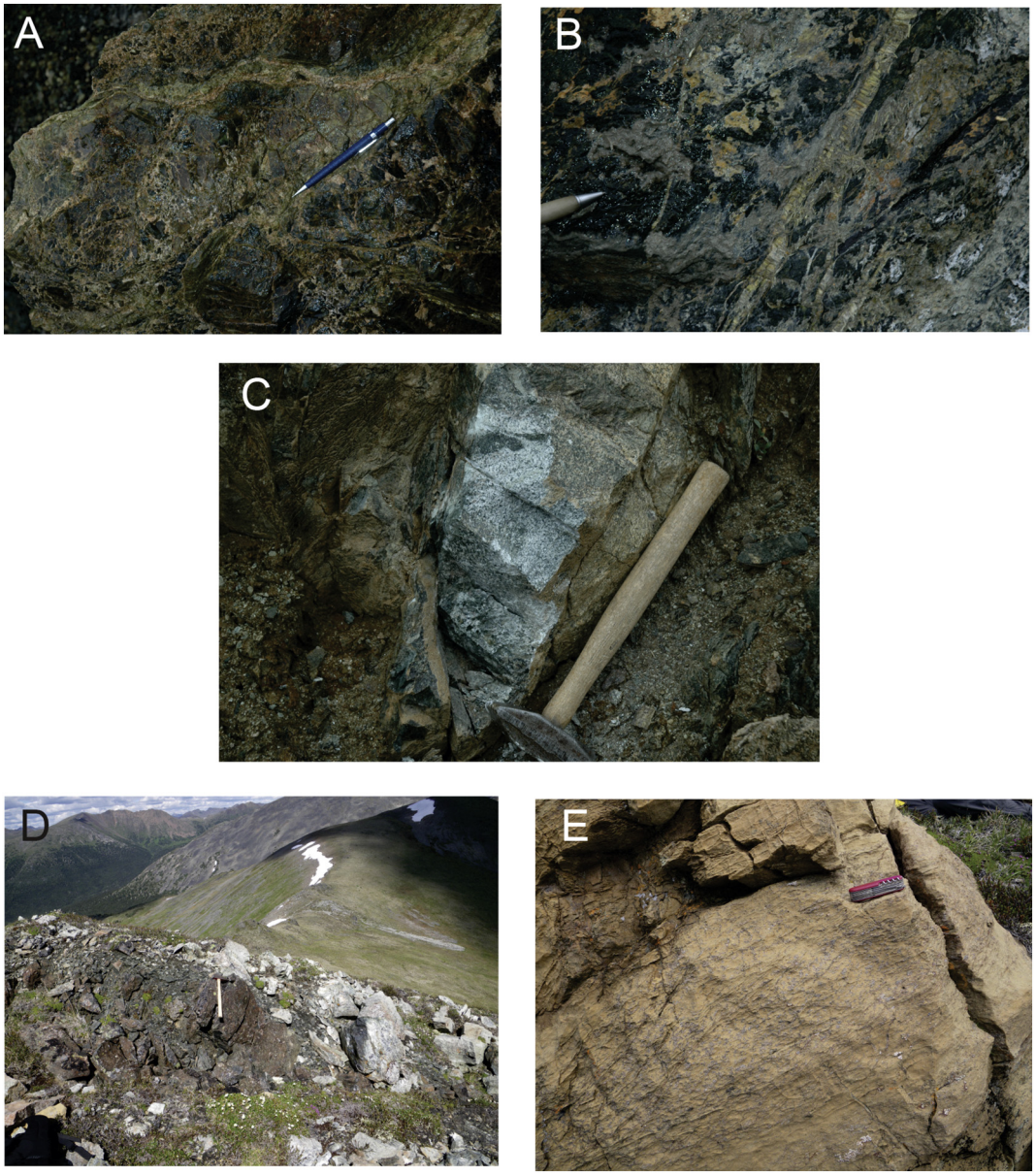

Fig. 4. A. Strongly serpentinized and listwanitizised Clinton Creek ultramafic rocks; B. Close-up of altered pegmatitic leucogabbro that has intruded serpentinite of Clinton Creek complex. Gabbro itself also altered to chlorite and carbonate and cut by serpentine veins; C. Leucogabbro intrusion into the Midnight Dome serpentinized ultramafic complex. Gabbro displays a weak foliation. D. Leucotonalite cutting harzburgite of E and pyroxenite dike. The pyroxenite in turn cuts the serpentinized harzburgite. E. Same location as D. Foliated and lineated St. Cyr serpentinized harzburgite in part defined by a shape fabric of bastite pseudomorphs after orthopyroxene and chromite aggregates.

mantle tectonite, cumulate ultramafic-mafic rocks, isotropic gabbro, sheeted dikes, pillow basalt and pelagic-hemipelagic sediment (Anonymous, 1972) have not been recognised here or elsewhere in the SMT by us or previous workers (e.g. Piercey et al., 2012; Parsons et al., 2018a). Notably, sheeted dikes are poorly developed or missing altogether, ultramafic rocks are abundant, and the volume of crustal mafic igneous rocks is commonly subordinate to the associated ultramafic rocks. This suggests that these oceanic rocks formed in a ridge environment where spreading was predominantly accommodated by tectonic extension, either due to localization of strain and/or lower magma productivity than typical Penrose-type ophiolites (e.g., Robinson et al., 2008). That is, spreading in these complexes was likely slow and largely accommodated by exhumation of lower-crustal and/or upper-mantle rocks to shallow crustal levels and locally onto the seafloor along large-scale, shallowly dipping detachment faults, forming ocean core complex(s) (e.g., Schroeder and John, 2004; MacLeod et al., 2009; Miranda and Dilek, 2010; Tani et al., 2011). This setting is typically characterised by emplacement of gabbro into exhumed mantle sections, limited basaltic magmatism and formation of active fault scarps exposing mantle rocks to mass wasting during eruption of the overlying basalts. Permian conglomerates and ophicalcites containing serpentinite and gabbro have been identified in correlative SMT ophiolites in the Sylvester allochthon in British Columbia (Nelson, 1993; Roback et al., 1994; Ryan et al., 2015) and are consistent with this scenario.

Ocean core complexes are now recognised to be common in continent to ocean rifts (e.g., Manatschal et al., 2011), slow to oblique spreading mid-oceanic ridges (e.g., MacLeod et al., 2009) and backarc spreading centres (e.g., Ohara et al., 2003; Tani et al., 2011), and they form a major component of several suprasubduction zone ophiolite belts (e.g., Tremblay et al., 2009; Miranda and Dilek, 2010). Limited analyses of tholeiitic mafic plutonic rocks of the Midnight Dome and

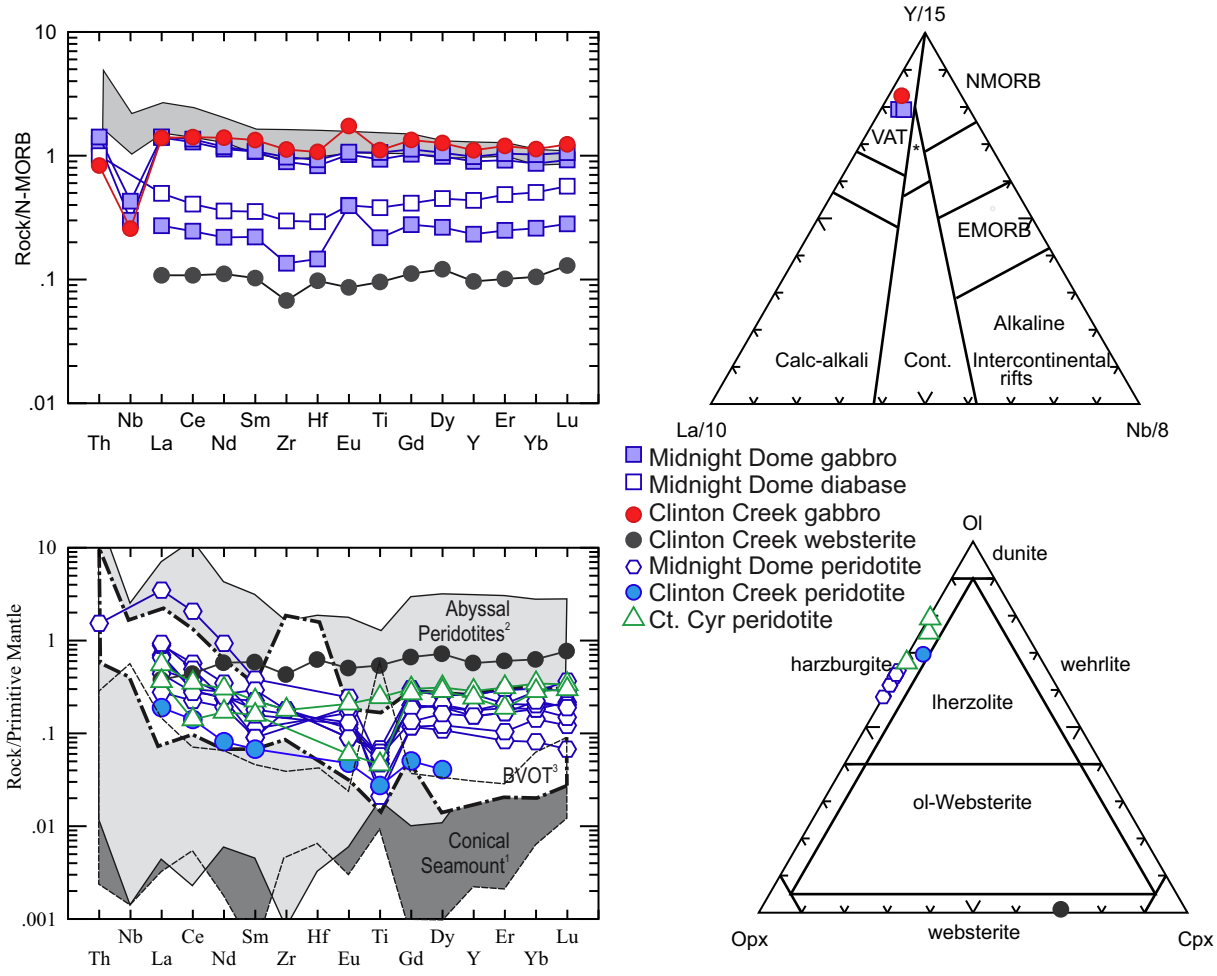

Fig. 5. Geochemical characteristics of the Clinton Creek, Midnight Dome and St. Cyr complexes. A. N-MORB normalized (Sun and McDonough, 1989) multi-element diagram of mafic rocks. Websterite plotted for reference. Composition of Cretaceous basalts (mainly sheet flows) erupted along the distal part of the hyperextended Newfoundland margin (ocean-continent transition) are plotted in the grey band (Robertson, 2007) for reference. B. Tectonic setting discrimination plot of mafic rocks (Cabanis and Lecolle, 1989). C. Primitive mantle normalized (Sun and McDonough, 1989) multi-element diagram of ultramafic rocks and comparison to peridotites from known tectonic settings (1 – Savov et al., 2005; 2- Niu et al., 2004; 3 – Baie Verte Oceanic Tract (BVOT) – Bedard and Escayola, 2010). D. IUGS modal classification of ultramafic rocks.

Clinton Creek complexes (Fig. 5, Table 2) are consistent with formation in a supra-subduction zone setting as indicated by strong Nb depletion (e.g., Cabanis and Lecolle, 1989; Pearce, 2014). Similarly, major element chemistry and Cr-spinel composition from the ultramafic rocks suggests a high degree of depletion typical of peridotites in arc settings (Fig. 6). LREE enrichment in harzburgite may indicate post-melt extraction enrichment, likely due to late stage melt percolation through exhumed and cooled peridotite at shallower depth; however, as similar enrichment has been observed in both forearc (Bedard and Escayola, 2010) and abyssal peridotites (e.g., Niu et al., 2004), this is not diagnostic of tectonic setting.

Gabbroic rocks from the Clinton Creek and Midnight Dome complexes yielded overlapping within-error middle Permian U-Pb zircon ages (264 ± 4 Ma and 265 ± 3 respectively) indicating broadly coeval formation (Fig. 3) in a similar tectonic setting based on the overall geochemical characteristics. Gabbroic rocks intimately associated with ultramafic bodies elsewhere in the SMT also yielded similar radiometric ages, which mainly range between 275 and 260 Ma (Fig. 1; Gabrielse et al., 1993; Nelson and Bradford, 1993; Colpron et al., 2006a; Murphy et al., 2006; Parsons et al., 2018a). Based on these age constraints we infer that spreading and mantle exhumation occurred throughout the SMO at ca. 265 Ma.

The felsic leucotonalite-trondhjemite intrusive bodies in the ultramafic rocks of the St. Cyr klippe yielded an age of 309 ± 5 Ma (Fig. 3) and provides a minimum age of mafic magmatism, since no evidence of a consanguineous relationship between the felsic and mafic igneous rocks exists at present. The age of the intrusive felsic magmatism, suggest a relationship to the juvenile Klinkit arc cycle, provided that the tuffaceous rocks of the Klinkit Group are as old as Pennsylvanian as is generally inferred (Roots et al., 2006; Simard et al., 2003; Piercey et al., 2006). The age of the Klinkit Group tuffaceous rocks, the principal representative of the Klinkit arc cycle, is solely constrained by a U-Pb age of ca. 281 Ma from an andesitic tuff of the upper part of the Butsih Formation (Roots et al., 2002, 2006). The ultramafic-mafic complex of the St. Cyr klippe is thus older than those present in the Midnight Dome, Clinton Creek, Dunite Peak, Campbell Range Formation and the Sylvester allochthon and represents an earlier rifting event in the SMO. Considering its association with Late Devonian (ca. 373 Ma) or older oceanic-like mafic rocks (Fallas et al., 1998), it may be a correlative of the ophiolitic ultramafic-mafic body in the Klatsa metamorphic complex (Devine et al., 2006) and represent another slice of Late Devonian transitional oceanic lithosphere.

6.1. *Origin of middle Permian ultramafic-mafic complexes*

Previous geochemical studies of SMT mafic rocks in the Finlayson

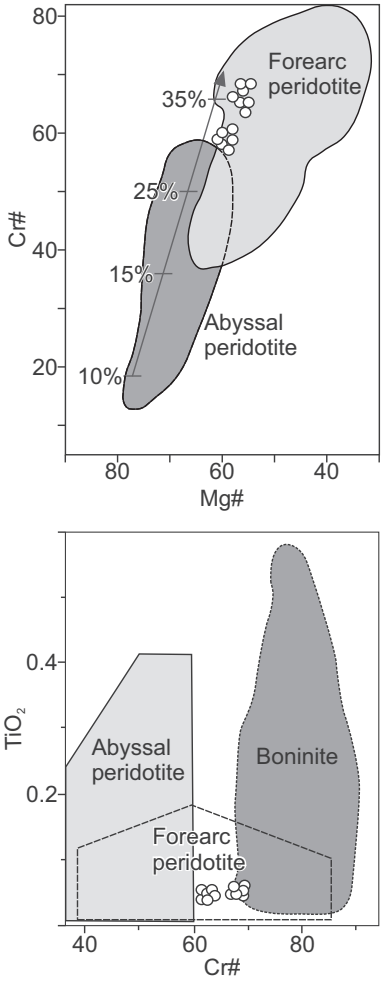

Fig. 6. Chromian spinel discrimination plots of peridotite in Midnight Dome complex.
(Modified from Dick and Bullen, 1984.)

area lacked the resolution of trace elements to effectively differentiate IAT from MORB lavas (e.g., Plint and Gordon, 1997). On the basis of their Ti-V data, SMT in the Finlayson area are predominantly ocean floor basalts similar to some SSZ ophiolites (Pearce, 2014). Correlative rocks include a mixture of MORB and IAT (Colpron et al., 2005; Parsons et al., 2018a). Marine basalts from the Sylvester allochthon in British Columbia also comprise a mixture of MORB and IAT. The IAT chemistry of the mafic rocks and highly depleted nature of the ultramafic rocks suggests a subduction zone-modified mantle for the SMT mafic-ultramafic complexes.

Subduction zone-modified mantle source can be either due to subduction coeval with emplacement of magmas or, less commonly, it can be inherited from a previous period of subduction-related melting and metasomatism. For example, Cretaceous hyperextension of the Newfoundland margin of the Atlantic Ocean resulted in exhumation of highly depleted spinel harzburgite subcontinental mantle lithosphere and emplacement of backarc-like magmas; however, the suprasubduction zone signature is most likely related to the closure of pre-Mesozoic oceans (Robertson, 2007). Similarly, the Woodlark basin in the southwest Pacific is characterised by both MORB and arc-like magmas, suggesting inheritance from earlier subduction (Perfit et al., 1987). The mixture of MORB and IAT magmas in the Permian ophiolite complexes thus presents a challenge regarding interpretation of their tectonic setting solely based on geochemistry. The regional distribution of arc signatures in the SMT, their dominantly Permian age, as well as their structural emplacement above the YTT and the Laurentian margin (e.g., Plint and Gordon, 1997; Canil and Johnston, 2003; Petrie et al., 2015; Parsons et al., 2018a) suggest that these ophiolite complexes did not form part of the subducting SMO floor or any other oceanic basin they may have formed in. Thus, these ophiolites did not form during rifting of YTT from Laurentia and subsequent spreading related to opening of the SMO. Rather we interpret them to have been part of an arc-backarc system formed during the oceanic basin's closure, which subsequently was obducted onto YTT. The Permian SMT arc-backarc rocks were referred to by Parsons et al. (2018a) as the Dunite Peak oceanic arc.

6.2. Permian setting of the YTT

The new and existing ages of ultramafic-mafic complexes in the SMT tightly constrain an important middle Permian event generating SSZ magmatism adjacent to the YTT. This event was broadly coeval with Permian deformation, metamorphism, exhumation and magmatism in the YTT, where the early Permian part of the juvenile Klinkit Arc phase of magmatism (281 ± 2 Ma, Roots et al., 2002, 2006; Colpron et al., 2006b) was followed by ca. 275–260 Ma blueschist to eclogite facies metamorphism of the YTT (Creaser et al., 1997b; Fallas et al., 1998; Petrie et al., 2015, 2016; Gilotti et al., 2017). The locus of the eclogite metamorphism approximately coincides with the SMT-YTT boundary (Fig. 1; Gilotti et al., 2017). Development of eclogite within the YTT basement was closely followed by structural emplacement of small orogenic peridotite bodies at ca. 262 Ma into the YTT basement (Buffalo Pitts peridotite: Canil et al., 2003; Johnston et al., 2007). The exhumation of orogenic peridotite was interpreted to have occurred as a result of relatively magma-poor hyperextension of continental crust located in a backarc setting of the east-facing middle Permian YTT Klondike arc (Canil et al., 2003; Johnston et al., 2007). The associated gabbroic rocks were interpreted to provide a minimum age for the structural emplacement of the mantle rocks in the crust and/or onto the seafloor (Reston and Manatschal, 2011), because they represent small batches of mafic melt generated during or shortly after exhumation (e.g., Jagoutz et al., 2007). Hyperextension was accompanied and followed by calc-alkaline felsic magmatism that involved crustal anatexis of YTT basement (ca. 265 to 257 Ma: Ruks et al., 2006), sparse peraluminous magmatism (ca. 252 Ma: Beranek and Mortensen, 2011) and high-grade metamorphism (ca. 239 Ma: Berman et al., 2007). The chronology of these middle to late Permian events suggests a period of major tectonic reorganization in the YTT and adjacent terranes.

7. Evaluation of tectonic models

Any tectonic model that is proposed for the setting of the Clinton Creek and Midnight Dome complexes needs to address Permian subduction in the SMO, suprasubduction zone chemistry of the Clinton Creek and Midnight Dome complexes, obduction rather than subduction of Clinton Creek, Midnight Dome and related SMT ophiolite complexes, the spatially nearly coincident location of Permian and Mississippian eclogite-facies metamorphism, and broadly coeval exhumation of orogenic peridotites. Existing tectonic models (e.g. Piercey et al., 2006; Berman et al., 2007) do not adequately address all of these nearly coeval Permian events in a single tectonic framework. Hence, in the following sections we evaluate existing models and explore alternative tectonic scenarios based on modern and recent analogues in the southwest Pacific. We utilize the Taiwan collision zone, where part of the Luzon arc is presently colliding with the South China Sea continental margin (e.g., McIntosh et al., 2005), as a geometrical analogue for the oldest and most speculative parts of our models (Figs. 7, 8). The use of this analogue allows our framework to start with a tectonically reasonable configuration. From this initial configuration we explore possible tectonic scenarios that could, in principle, explain the observed relationships. We discuss multiple tectonic scenarios in order to demonstrate that existing tectonic models which treat YTT as a singular terrane are difficult to reconcile with the existing constraints (Fig. 7).

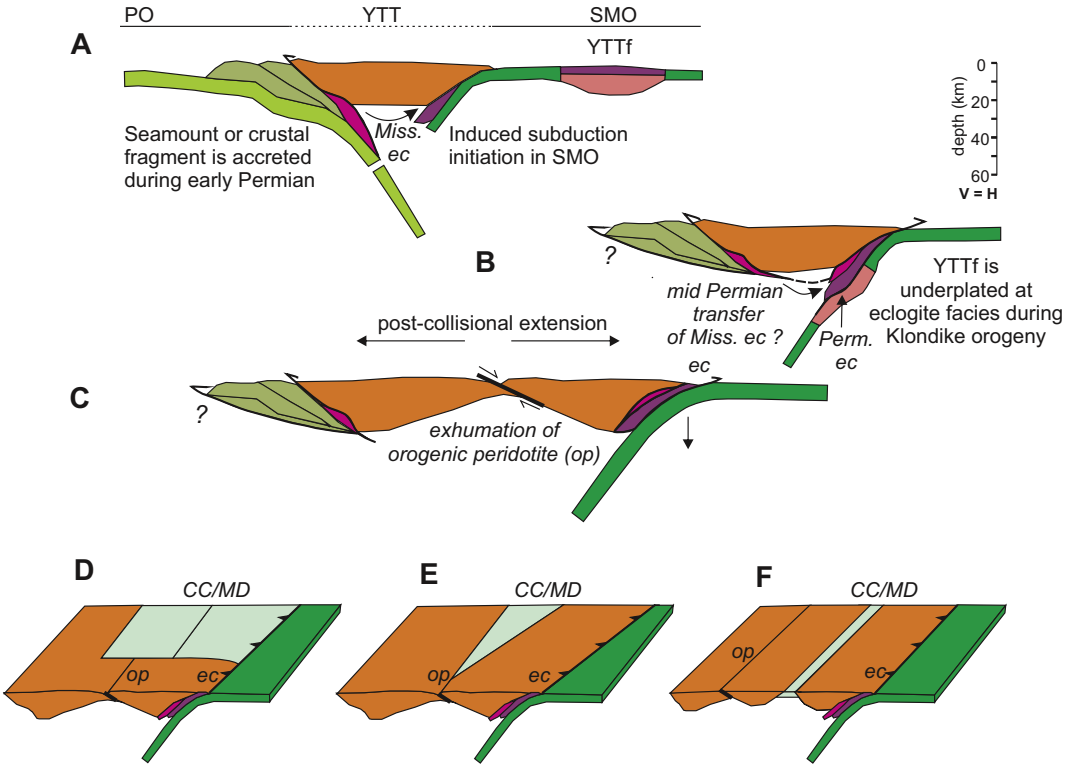

Fig. 7. Yukon-Tanana (YTT) as a singular late Paleozoic terrane. YTT is in the upper plate during both Late Devonian-early Permian subduction of the Panthalassa Ocean (PO) and early-late Permian subduction of the Slide Mountain Ocean (SMO) following a subduction polarity reversal. A. Collision of seamount or crustal ribbon terminates east-dipping subduction beneath YTT and induces subduction in the SMO. Mississippian eclogite formed during east-directed subduction and incorporated in a west-facing subduction complex. Following early Permian collision with an outboard terrane (not preserved?), the Mississippian eclogite and parts of the host subduction complex were progressively emplaced further to the east beneath the eastern (backarc) edge of the YTT arc as a result of forearc subduction (process based on Sajona et al., 2000; McIntosh et al., 2005). B. Tectonic capture of the Mississippian eclogite and incorporation in an east-facing Permian subduction complex following initiation of a west-dipping subduction zone in the SMO, which leads to its subsequent juxtaposition with Permian eclogite. The Permian eclogite formed by partial subduction of a small continental ribbon fragment (YTTf, see also Fig. 2) or as a result of subduction erosion (Gilotti et al., 2017). C. Subduction rollback drives asymmetrical extension and exhumation of orogenic peridotites (op) in YTT (upper plate) immediately after underthrusting and formation of eclogite. D–F. Possible relationships between orogenic peridotite (op) and Clinton Creek (CC) and Midnight Dome (MD) complexes following the initiation of subduction in the SMO. D. Clinton Creek-Midnight Dome spreading centre is located in YTT re-entrant and propagates into YTT leading to continental rifting and exhumation of Buffalo Pitts orogenic peridotites (Johnston et al., 2007). Permian eclogite is exhumed in the subduction channel along the YTT promontory. E. Asymmetrical rifting leads to orogenic peridotite exhumation and ophiolite formation along strike. F. Orogenic peridotites are exhumed along a separate rift from the ophiolites.

We then explore the possibility that YTT is a composite terrane that formed by amalgamation of juvenile oceanic and continental fragments in the Permian (Figs. 8, 9). The various plate tectonic configurations that can create an YTT composite terrane are guided by the relationships in the Australia – Pacific boundary zone in Papua New Guinea (Fig. 10).

7.1. YTT as a singular terrane

Most recent models (Mortensen, 1992; Nelson, 1993; Piercey et al., 2006; Pecha et al., 2016 and references therein) assume that the present distribution of terranes is indicative of their original relative position and polarity of juxtaposition in the Late Paleozoic and Early Mesozoic, despite the complex structural overprint related to Jurassic to Cretaceous shortening and exhumation (e.g., Staples et al., 2016; Joyce et al., 2015) and Cretaceous strike-slip translation (e.g., Gabrielse et al., 2006). In these models the YTT arc-backarc terrane formed above an east-dipping subduction zone and separated from Laurentia during the Famennian-Early Mississippian, opening the SMO. Subsequently a subduction polarity flip initiated Permian subduction in the SMO (e.g. Devine et al., 2006; Piercey et al., 2006; Berman et al., 2007), although the cause of the cessation of east-directed subduction and the reversal of subduction polarity was not identified (see Fig. 2).

Subduction polarity flips generally require a collision (see above), hence the postulated east-dipping subduction should have been terminated by accretion of an as yet unidentified plateau, arc or microcontinent (Fig. 7a). Evidence for such a collider is not preserved, but Famennian-Mississippian deformation, metamorphism and an unconformity in YTT (Gabrielse et al., 1993; Colpron et al., 2006a, 2006b; Mihalynuk et al., 2006; Murphy et al., 2006; Roots et al., 2006; Devine et al., 2006; Berman et al., 2007; Ryan et al., 2015) may be related to such a collision. The strong Mesozoic tectonic and metamorphic overprint, including large tangential translations could have removed or masked a collider. Such a collision could be responsible for the Mississippian eclogite-facies metamorphism of parts of the downgoing lower plate (Erdmer et al., 1998; Devine et al., 2006). Rocks of the upper plate could also reach eclogite-facies conditions if rocks of the arc-trench gap are subjected to subduction erosion and/or partially subducted and underplated during collision (Fig. 7a; e.g., McIntosh et al., 2005). Partial subduction of the forearc during collision is consistent with the arc-like geochemical characteristics of the Mississippian eclogite (Creaser et al., 1999). Previous models exhumed and then transported the Mississippian eclogite and associated Klatsa complex rocks over the associated arc towards the Permian foreland to finally emplace it along the eastern margin of YTT near its tectonic contact with the Laurentian margin (Fig. 2; Devine et al., 2006; Berman et al., 2007). This is a tectonically complicated and unlikely scenario (Fig. 2) because it involves exhumation of the Mississippian eclogite and associated rocks in

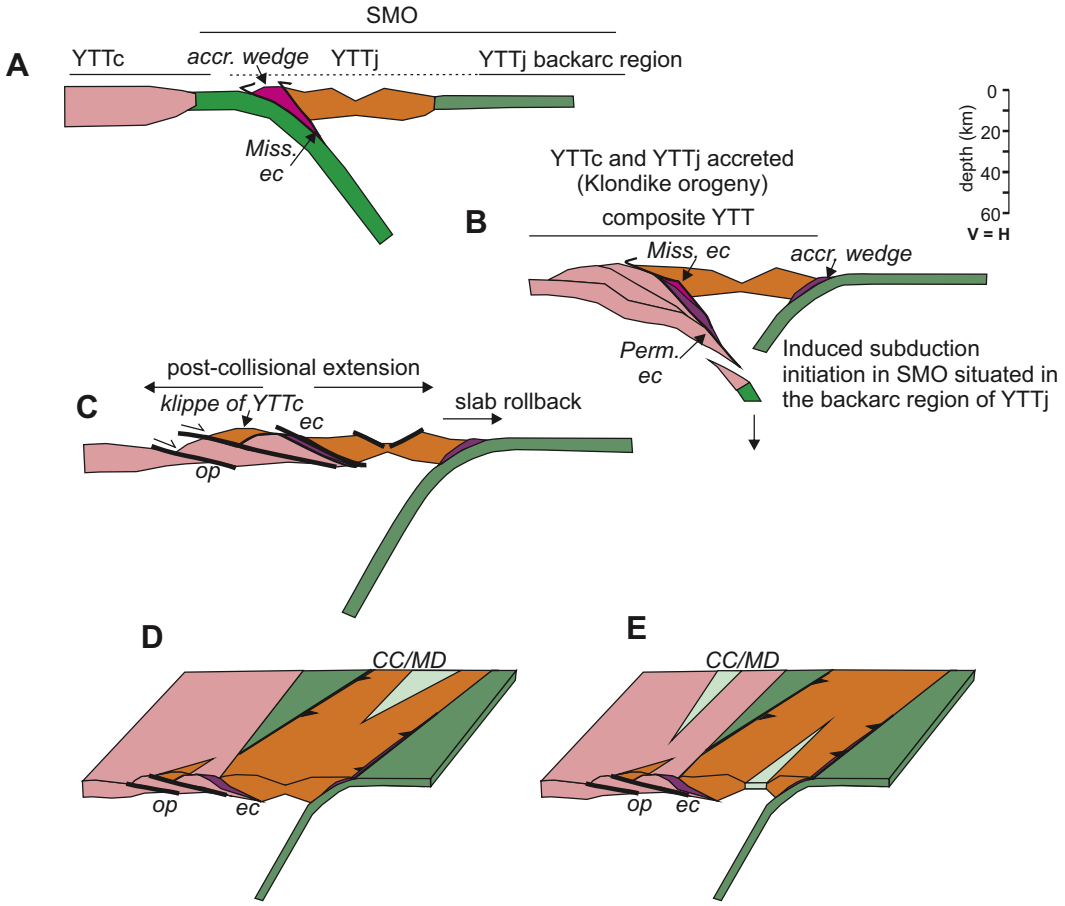

Fig. 8. YTT as a composite terrane. Late Paleozoic tectonic configurations of the Yukon-Tanana microcontinent (YTTc) and the converging oceanic arc-backarc terrane (YTTj) after initiation of east-directed subduction beneath YTTj during the Mississippian or earlier, modified and expanded from Parsons et al. (2018a). A. Subduction initiation beneath YTTj leads to formation of Mississippian eclogite (see text). B. Middle-late Permian collision (Klondike orogeny) between YTTj and YTTc leads to partial subduction of the leading edge of the YTTc, formation of Permian eclogite and juxtaposition with the Mississippian eclogite near the suture following exhumation. The YTTj-microcontinent (YTTc) collision is followed by a subduction polarity flip and initiation of west-directed subduction in the remaining part (backarc region of YTTj) of the SMO. C. Post-collisional extension driven by slab rollback results in exhumation of orogenic peridotite (op) and post-collisional magmatism. D. The relationship between ophiolites and orogenic peridotites can be explained by diachronous collision, such that orogenic peridotite is exhumed in already collided part of the orogen whereas YTTj is rifting where the collision has not yet occurred. As a result the subduction polarity reversal is accordingly diachronous (van Staal et al., 1998, Fig. 6). E. Similar to D but non-cylindrical, asymmetrical rifting in YTTc leads to ophiolite formation along strike of where orogenic peridotite is exhumed. The final configuration of the eclogites, YTTc and possible remnants of accreted of ocean floor rocks in SMT is mainly a result of Mesozoic shortening and extension (see Fig. 9c and text).

the forearc, the cause of which is unclear, followed by retro-arc-directed thrusting prior to the initiation of west-directed subduction in the SMO (Devine et al., 2006). Hence, this would cause significant burial of a still hot and possibly still magmatically active arc segment without causing a magmatic and/or high-temperature metamorphic overprint in the overthrusted eclogite-bearing allochthon.

The Taiwan collision zone, where the Luzon arc has overthrust its own forearc (e.g., McIntosh et al., 2005), shows a less complicated, albeit speculative, alternative. In this setting eclogite generated in forearc rocks can be transferred beneath the arc instead by underthrusting at depth into the backarc region (Fig. 7a, b). The Luzon arc is only ~25 km across in the collision zone (see Fig. 12, Line 23 in McIntosh et al., 2005), and any post-collisional rebound and/or tectonic exhumation could result in emplacement of parts of the partially subducted forearc block into the former backarc region. Ultimately, the continued convergence across the collision zone within YTT would induce subduction in the backarc region (Fig. 7a; e.g., Pubellier et al., 1999; Taira et al., 2004), thus initiating west-dipping subduction of the SMO inboard of YTT and exhuming the eclogites in the new subduction channel.

During west-directed subduction of the SMO, the YTT became the site of an early-middle Permian arc built upon the Snowcap siliciclastic substrate in the existing tectonic models (Colpron et al., 2006b; Piercey et al., 2006). By middle Permian, parts of the YTT were subjected to eclogite and blueschist facies metamorphism (275–260 Ma; Fallas et al., 1998; Erdmer et al., 1998; Creaser et al., 1999; Petrie et al., 2015; Petrie et al., 2016; Gilotti et al., 2017; Colpron et al., 2017). Since all phases of the early-middle Permian arc are interpreted to be built upon the YTT (Colpron et al., 2006b; Piercey et al., 2006; Gilotti et al., 2017), this requires that the upper plate was partly subducted, possibly for a second time. Mississippian tonalite and granite within YTT associated with the Permian eclogites were subjected to coeval high-pressure metamorphism (Petrie et al., 2015; Gilotti et al., 2017; Colpron et al., 2017), which suggests that these arc-like rocks and their Snowcap substrate were subducted together. Potential causes for this can include (i) YTT rocks were dragged into the subduction channel during subduction initiation in the SMO, forearc block underthrusting and/or during subduction erosion (Gilotti et al., 2017) that led to high pressure metamorphism by middle Permian (Fig. 7a); or (ii) a buoyant microcontinent calved off of YTT was partly subducted and underplated (Figs. 2, 7b; e.g., Devine et al., 2006). Continued subduction of the SMO and slab-rollback subsequently must have induced extension of the YTT

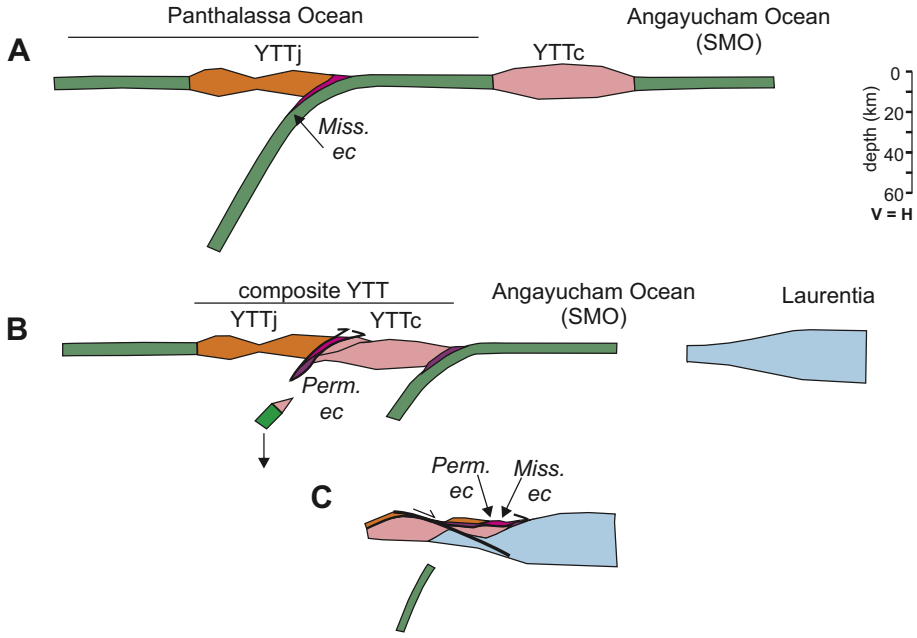

Fig. 9. A. Formation of an oceanic arc-backarc complex (YTTj) outboard in the Panthalassa Ocean as a result of west-directed subduction. B. Obduction of YTTj onto YTTc during the Klondike orogeny, followed by stepping-back of subduction in the SMO or Angayucham Ocean. The processes discussed in Fig. 8 to account for exhumation of orogenic peridotite and post-collisional magmatism are principally the same. C. Further east-directed translation of the YTTj and eclogites above YTTc and Laurentia took place during the Jurassic-Cretaceous. The final present day configuration with the SMT rocks outlining the contact between Laurentia and composite YTT is principally a product of Mesozoic and later thrusting and exhumation.

and resulted in broadly coeval exhumation of eclogite in the forearc and exhumation of orogenic peridotite in the backarc (Fig. 7c; Johnston et al., 2007).

The large number of age constraints indicate that the change from eclogite formation/exhumation, exhumation of orogenic peridotites to formation of the Clinton Creek and Midnight Dome ophiolite complexes was very rapid, possibly as short as 2 my. The Clinton Creek and Midnight Dome and correlative SSZ ophiolite complexes in the SMT must have occupied an upper plate setting (see previous) and did not form part of the subducting SMO floor. These relationships require a complex tectonic configuration between ca. 275 and 260 Ma. There are several types of configurations that could in principle explain these relationships, including (i) ocean-continent transition within the arc (Fig. 7d), (ii) propagating backarc rift in a continental arc (Fig. 7e), and (iii) discrete continental backarc rift, oceanic backarc and arc (Fig. 7f). Presence of an ocean-continent transition within the YTT (e.g., Mortensen, 1992) could have resulted from an original promontory – re-entrant configuration inherited from its rifting from the Laurentian margin. This configuration could explain exhumation of orogenic peridotite in continental basement on-strike with formation of an oceanic spreading centre (Fig. 7d; e.g., Davey et al., 2016). A similar along-strike relationship can be achieved by a propagating rift model, where oceanic crust is formed in areas with the greatest degree of extension on-strike with continental rifting (Fig. 7e; e.g., Taylor et al., 1999). Alternatively, orogenic peridotites may have been exhumed along a separate rift segment further in the backarc or along the margins of the rift (Fig. 7f; e.g., Canil et al., 2003; Johnston et al., 2007). This complex arc-backarc system would continue to develop above the subducting SMO until collision with and emplacement of YTT onto the Laurentian margin.

Modifying the existing models by introducing a Mississippian collision, emplacing Mississippian eclogite under the arc (Fig. 7a) and placing the suprasubduction zone Permian ophiolites into the upper arc plate (Fig. 7d–f) does improve the viability of the tectonic models as there are modern examples where such processes occur. However, this modification still requires several unusual tectonic circumstances such as lack of preservation of an obvious Late Devonian-Early Mississippian collider, coincident exhumation and emplacement of Mississippian and Permian eclogites, which allegedly formed on opposite sides of a continental arc system and partial subduction of parts of the upper plate arc terrane to eclogite facies at two separate times. Although all of these processes are plausible on their own in principle, their juxtaposition in one terrane is rather improbable. In addition, these models still require subduction in the Permian backarc oceanic basin (SMO), represented by Clinton Creek, Midnight Dome and correlative ophiolites, and thus not do not resolve the problem of obducting ophiolites from the subducting plate. Other tectonic models should therefore be considered (e.g. Parsons et al., 2018a), which are discussed below.

7.2. YTT as a composite terrane

As discussed above, the YTT is generally viewed as a single terrane characterised by multiple superposed magmatic cycles interpreted as arcs (see Colpron et al., 2006b; Piercey et al., 2006; Nelson et al., 2006 and references therein). One of the major weaknesses of this model is that it requires formation of alternating juvenile oceanic-like arc and continental magmatic suites above the same YTT continental basement. This continental basement must have undergone significant degrees of extension throughout its history as indicated by an abundance of tholeiitic and alkalic igneous rocks and close spatial links with ophiolitic rocks of various ages (e.g., Piercey et al., 2001, 2006, 2012; Simard et al., 2003; Murphy et al., 2006; Petrie et al., 2015, this paper). Specifically formation of ophiolites and juvenile arc magmatism (e.g. 314–269 Ma Klinkit cycle) suggest that the YTT continental crust had fully rifted, precluding preservation of significant continental basement inferred to be present beneath all of YTT's Snowcap assemblage (Piercey et al., 2006; Piercey and Colpron, 2009). Hence, formation of a subsequent continental arc cycle (e.g. 269–253 Ma Klondike cycle) above Snowcap Assemblage rocks either requires that the Klondike cycle magmatism formed in an unrelated tectonic setting and/or different plate, or that juvenile and continental domains were tectonically juxtaposed prior to the Klondike cycle magmatism. The latter is in our opinion a more viable hypothesis. That is, YTT formed by amalgamation of a microcontinent and an intraoceanic arc-backarc terrane and then subsequently evolved as a composite terrane (Parsons et al., 2018a). The dated, 309 Ma leucotonalite-trondhjemite in the St. Cyr klippe is consistent with this hypothesis, because it may correspond in age with the juvenile Klinkit arc cycle (Simard et al., 2003; Piercey et al., 2006), yet intrudes into an oceanic assemblage represented by serpentinitized harzburgite, pyroxenite and gabbro. We emphasize that the association and/or interaction of arc magmatic cycles with Snowcap Assemblage rocks does not exclude formation of the arc rocks in an

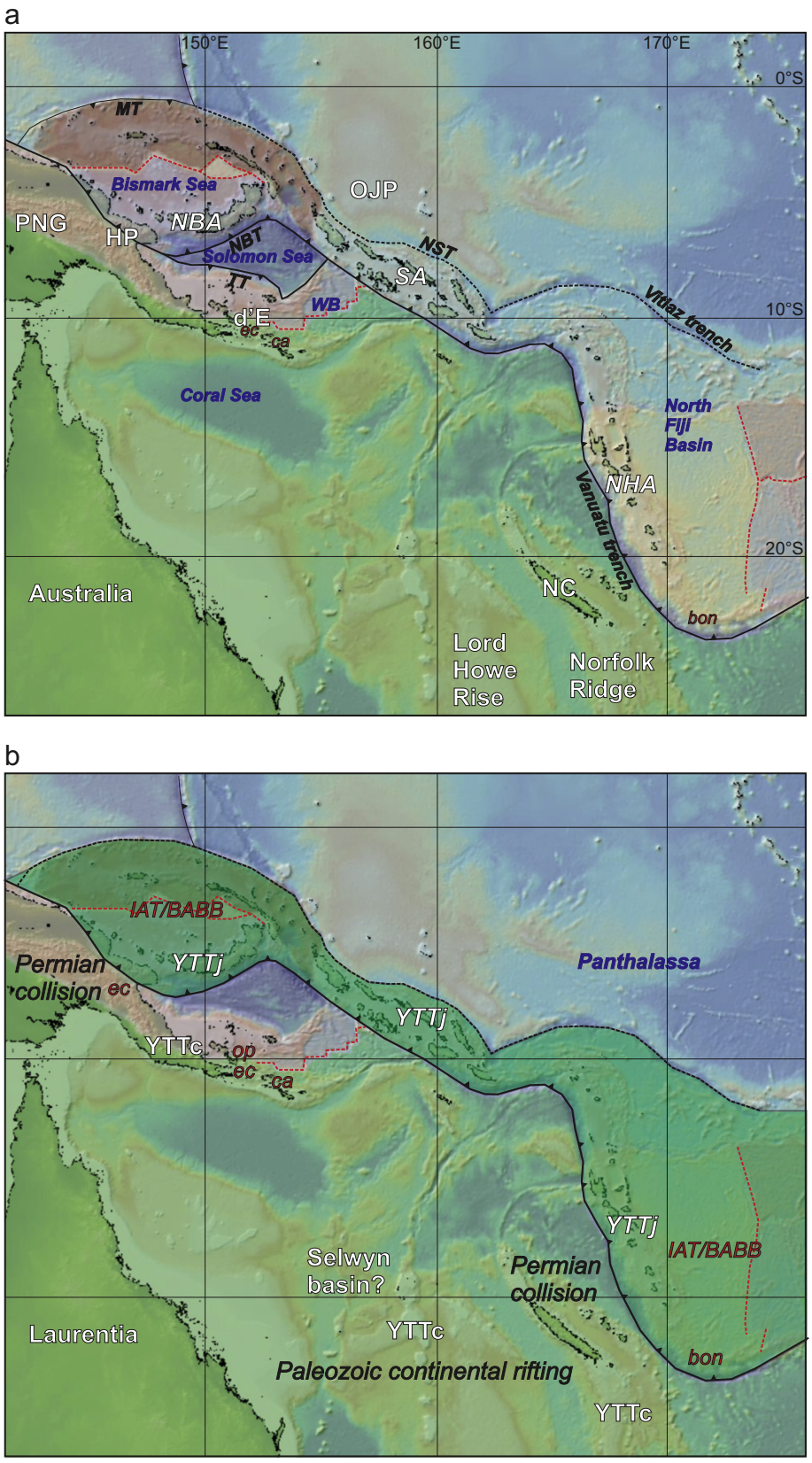

Fig. 10. A. Simplified geology of the Australia – Pacific plate boundary zone. Background image is generated from http://www.geomapapp.org. Collision between Australia and the New Britain arc (NBA) in Huon Peninsula (HP) propagates towards the east progressively closing the Solomon Sea. The Woodlark basin (WB) is actively spreading and propagating into Australian crust in eastern Papua New Guinea (PNG). Here exhumation of eclogite (ec) and calc alkaline magmatism (ca) has occurred recently in the d'Entrecasteaux Islands (d'E). The Woodlark Basin spreading centre is subducted beneath the Solomon Arc (SA) at its eastern edge. Stippled line is the now inactive North Solomon Trench (NST), which accommodated convergence between the Solomon arc and Ontong Java plateau (OJP) until the subduction polarity reversal and formation of the New Britain Trench (NBT) and its extension to the southeast (South Solomon Trench). New Caledonia (NC) and Norfolk Ridge are going to collide with the New Hebrides Arc (NHA) in the future, juxtaposing NHA boninites (bon) with rifted continental margin rocks. B. Elements of Laurentia and Yukon Tanana composite terrane superimposed on the Australia – Pacific plate boundary zone. In this analogy, Australia is Laurentia, the New Britain-Solomon arc backarc system is YTTj, which is mainly characterised by IAT and BABB rocks; YTTc are the continental ribbons such as Lord Howe rise and Norfolk ridge. The intervening basin between the Lord Howe Rise and Australia could be analogous to the Selwyn basin. In this analogy, the diachronous collision, outlined in eastern New Guinea is not between Laurentia and the YTT, but between YTTc and YTTj. EC, OP and CA are exhumed eclogite, orogenic peridotite and calc-alkaline magmatism respectively generated as a result of rifting propagating into the Permian collision zone between YTTj and YTTc. MT, Manus Trench; TT, Trobriand Trough.

intra-oceanic setting in the SMO (cf. Colpron et al., 2006a). The youngest component of the Snowcap assemblage rocks could have been deposited in this basin during the early stages of SMO development. Extensional allochthons with a Snowcap assemblage cover, isolated within a progressively widening SMO (cf. Manatschal et al., 2006; Mohn et al., 2010) locally could have become basement to subsequent arc volcanism (see Roots et al., 2006) following subduction initiation in SMO and thereby cause zircon inheritance in otherwise intra-oceanic

rocks. Continental sources have been detected, for example, in the oceanic Solomon arc based on inherited continental-derived zircons as old as Archean (Tapster et al., 2014).

The bulk of the continental YTT, which comprise the Snowcap Assemblage (e.g., Piercey and Colpron, 2009), Devonian to Early Carboniferous continentally contaminated magmatic rocks and Permian K-feldspar megacrystic (Klondike) intrusions and related volcanic rocks (Piercey et al., 2003, 2006; Ruks et al., 2006), are generally located to the west (outboard) of the juvenile arc volcanic rocks and ophiolites (Fig. 1; Colpron et al., 2016). For the following tectonic analysis, the continental part of composite YTT (YTTc), which is generally situated farthest to the west, will refer to continental rocks, including any accreted outboard blocks, while the 'oceanic' components of YTT (YTTj), which is generally situated more easterly will denote the juvenile arc-backarc volcanic rocks and associated SSZ ophiolitic rocks emplaced onto YTTc (Fig. 1). YTTj corresponds with the Dunite Peak oceanic arc terrane of Parsons et al. (2018a) and includes correlative SSZ ophiolitic rocks in the adjacent SMT such as the Clinton Creek and Midnight Dome complexes. The remnants of YTTj are now mainly preserved as relatively small klippes of oceanic crust and mantle above YTTc. Exhumation (e.g. Knight et al., 2013; Staples et al., 2016; Parsons et al., 2018a) has removed most of YTTj following its middle Permian to early Triassic obduction and subsequent Mesozoic thrusting and folding events (Figs. 8b, c and 9c; Berman et al., 2007). In this tectonic model, the YTT of Colpron et al. (2006a) is thus a composite terrane comprising at least two separate blocks (YTTc and YTTj) before their middle Permian-early Triassic amalgamation (Fig. 8a) and the present distribution of the YTT components is representative of their relative Permian paleogeographic position.

The juvenile, oceanic constituents preserved in the YTT of Yukon and northern British Columbia (YTTj) range in age from the Carboniferous to Permian (Murphy et al., 2006; Piercey et al., 2006), although some (e.g. ultramafic-gabbro complex of St. Cyr) may be as old as Late Devonian. However, many age constraints are based on regional correlations and presumed stitching relationships into assemblages of multiple rock units. For example, presence of unrecognised low-angle faults within the assemblages is suggested by juxtaposition of boninite with continental-rift related magmatic rocks (Piercey et al., 2012; Ryan et al., 2017) and structural emplacement of mantle rocks previously mapped as intrusions (Murphy et al., 2006; Piercey et al., 2006) into supracrustal sequences of the Finlayson district. Lack of recognition of such low angle faults makes several lithological correlations and stratigraphic interpretations suspect. We hypothesize that juvenile arc volcanic rocks, such as those present in the Klinkit Group (Simard et al., 2003; Piercey et al., 2006) represent the product of an extensional oceanic arc complex, which either initiated in the SMO, inboard of the composite continental YTTc block (Fig. 8a), along strike of YTTc or outboard of the YTTc (Fig. 9a). A Permian collision between YTTc and YTTj formed the YTT composite terrane and resulted in partial obduction of the oceanic YTTj, juxtaposition of Early Mississippian and Permian eclogite belts and initiation of west-dipping subduction east of the composite YTT by a Permian subduction polarity flip (Fig. 8b) as proposed by Parsons et al. (2018a). The arc-backarc rocks of YTTj do not necessarily comprise all of the preserved SMT. Early Permian and older occurrences of SMT, such as chert and associated mafic volcanic rocks (Nelson, 1993), may represent accreted remnants of ocean floor rocks from the oceanic basin in which YTTj originally formed.

Slab rollback following the subduction flip led to extension and exhumation of orogenic Alpine-type peridotite in the composite YTT and isolation of klippen of oceanic YTTj above continental YTTc (Fig. 8c). This composite arc system subsequently continued to develop above the west-dipping subduction zone progressively consuming the remaining vestige of the SMO until composite YTT's collision with and obduction onto the trailing eastern passive margin of the SMO, which started sometime after the Middle Triassic (Parsons et al., 2018a), possibly during the Early Jurassic (Evenchick et al., 2007).

The coeval exhumation of orogenic peridotites and emplacement of the Clinton Creek and Midnight Dome ophiolite complexes onto YTTc can be explained by the same along or across strike tectonic settings discussed above (Figs. 7d-f). However, the composite nature of the YTT in this model allows several additional tectonic scenarios capable of explaining formation of the Clinton Creek and Midnight Dome ophiolite complexes within the oceanic YTTj (Figs. 8d, e). A diachronous collision of the continental YTTc and oceanic YTTj blocks could result in extensional arc or backarc magmatism in the overriding oceanic YTTj, where the collision has not yet occurred, such that it is coeval with partial subduction of the continental YYTc to eclogite facies along strike where the collision already had started, and post-collisional extension along strike where the subduction polarity flip had occurred (Fig. 8d). The diachroneity of the collision may be due to oblique convergence or a marked promontory-re-entrant configuration of the margin of YTTc. The ongoing Luzon arc – China collision in central Taiwan, where a subduction polarity flip and collision are migrating diachronously from northeast to southwest in a geologically very short time frame is an example of such diachroneity (Huang et al., 2006).

The Clinton Creek and Midnight Dome ophiolite complexes form part of the overriding juvenile oceanic arc complex (YTTj) and do not represent normal oceanic lithosphere. In contrast to the singular YTT terrane model, this model is better at explaining the cause of the subduction flip, juxtaposition of continental and intraoceanic domains, isolation of ophiolites as klippes above YTT (e.g. St. Cyr klippe, Petrie et al., 2015; Dunite Peak, Parsons et al., 2018a; Harzburgite Peak complex, Canil and Johnston, 2003), juxtaposition of different ages of eclogite along the same boundary (Fig. 7b), and distribution of Carboniferous and Permian magmatism in distinct domains. Specifically, the Carboniferous-Permian oceanic arc complex (YTTj) is tectonically juxtaposed with a separate continental tectonic block (YTTc) (Fig. 8). As such, Carboniferous to Middle Permian arc magmatism is restricted to the overriding oceanic arc block (YTTj), whereas the Permian high grade metamorphism, crustal anatexis and post-collisional extension are generally restricted to the underthrusted continental YTTc block (e.g., Ruks et al., 2006; Berman et al., 2007). This is consistent with previous suggestions that Carboniferous arc rocks form a separate nappe within the composite YTT (e.g., Tempelman-Kluit and Wanless, 1980; Ryan et al., 2013a, 2013b; Ryan et al., 2014). The basal shear zone of this nappe, the Yukon River shear zone, could be a remnant of the original thrust along which YTTj was emplaced over YTTc during the late Permian-early Triassic (Parsons et al., 2018b).

In the composite YTT model, Permian eclogites could have formed by subduction of the leading edge of continental YTTc (Fig. 8b; Parsons et al., 2018a), including its entrained Mississippian tonalities and granite (Petrie et al., 2015; Colpron et al., 2017), partial subduction of a buoyant microcontinent calved off of YTTc (Fig. 2), or by subduction erosion of the YTTj forearc, which may have included some Snowcap Assemblage sediments and entrained intrusive rocks (Gilotti et al., 2017). However, the composite YTT model (Fig. 8) has a number of major drawbacks. Primarily it requires that subduction initiation in SMO (inboard of YTTc) had occurred during the Mississippian or earlier to account for eclogite formation at ca. 353 Ma (Erdmer et al., 1998; Devine et al., 2006) and its subsequent juxtaposition with the Permian eclogites (Fig. 8b, c). This implies that in the existing models subduction should have started immediately after the inferred Fammenian-earliest Mississippian rifting of YTTc from Laurentia, which in turn is mainly based on the occurrence of rift-related magmatism of this age in both terranes. Thus in the composite YTT model a separation of YTTc from Laurentia had to occur significantly earlier than the Famennian-earliest Mississippian, otherwise spreading in SMO could not be expected to generate enough oceanic lithosphere to sustain subduction for over 90 my. In addition, this model also requires that there was a significant volume of Laurentian derived sediment beneath the YTTj arc during the Mississippian phase of arc magmatism to explain the

evidence for crustal contamination in its rocks (Piercey et al., 2006). As such, we further explore the Permian aspects of this model in more detail on the basis of a comparison with the tectonic evolution of the Australia – Pacific plate boundary zone (e.g. Hall, 2002; Baldwin et al., 2012).

7.3. Comparison to modern tectonic configurations

Below we briefly discuss aspects of the tectonics of the Solomon Islands – Papua New Guinea region of the southwest Pacific (Fig. 10a), which we consider a viable modern analogue. Arc-collision, suprasubduction zone backarc spreading, rift-related magmatism and exhumation of eclogite recently took place coevally or nearly so and/or is still ongoing. The model that invokes two separate YTT building blocks (Fig. 8) and their Permian amalgamation has many analogies with the tectonic relationships observed here, although the Australian - Pacific plate boundary zone displays very complex relationships between continental slivers, arcs, ocean basins and arc-collisions in time and space. Potential configurations of the Laurentian margin, SMO, YTTj and YTTc could broadly correspond to the Australian margin, Solomon Sea, New Britain-Solomon-New Hebrides arc system and micro continental slivers such as the Lord Howe rise respectively. This area also provides a cautionary note on correlations of deformation, magmatism and metamorphism in older orogens based on age alone (cf. van Staal et al., 1998). For the purpose of discussion, we will concentrate on the relationships across the New Britain-Solomon-New Hebrides arc system (Fig. 10a). From east to west, the north-east facing phase of the Solomon arc was involved in a Miocene collision with the outboard oceanic Ontong Java Plateau in the now inactive North Solomon-Kilinailu subduction zone, leading to a subduction reversal in the Neogene (Mann and Taira, 2004; Taira et al., 2004). Although the Solomon island arc is considered intra-oceanic, it does contain Cretaceous to Archaean zircon xenocrysts, which suggest derivation from a continental source such as Australia (Tapster et al., 2014). This has implications for the interpretation of the oceanic YTTj block in that the presence of sparse inheritance continentally derived zircons in volcanic and plutonic rocks does not necessarily indicate an autochthonous stratigraphic relationship with the inferred continental YTTc substrate. No remnants of an Ontong Java-like oceanic plateau have been recognised in the composite YTT, although a collision between two buoyant blocks is a realistic mechanism to generate a subduction polarity reversal and induce subduction in a formerly opening oceanic basin.

Along-strike, the south-facing New Britain arc (Fig. 10a) is associated with normal subduction, whereas its westernmost segment has already collided with the Australian margin in the Finistere Range of the Huon Peninsula (Abers and McCaffrey, 1994). Further west along the Australian margin, arc polarity has switched to south dipping subduction along the west New Guinea trench. The collision between the Australian margin and the New Britain-Solomon arc system is diachronous, is propagating to the east, and will eventually lead to closure of the Solomon Sea. The Bismarck Sea, located in the backarc region of the New Britain Arc segment (Fig. 10a), is undergoing active spreading east of the collision zone near the Huon Peninsula. Hence, this zone is a realistic analogue for subduction polarity reversal overlapping with suprasubduction zone spreading and coeval arc-collision in the same tectonic system (Fig. 8d). We ignore the very slow, south-directed subduction along the Trobriand Trough along the south margin of the Solomon Sea as it only adds unnecessary complexity to this discussion. From west to east, the setting of the Australian continental margin changes from collision zone (with the western segment of the New Britain arc, Abers and McCaffrey, 1994; Galewsky et al., 1996), to a region of active continental rifting as a result of the westerly-propagating Woodlark rift along the eastern Papuan Peninsula (Fig. 10a). The latter rifting led to late Miocene exhumation of eclogite (Little et al., 2011; Baldwin et al., 2012; Webb et al., 2014). Further east, continental rifting has become fully oceanic in the Woodlark Basin (Taylor et al., 1999). The wedge-shaped spreading Woodlark Basin expands to the east and is here subducted under the Solomon Arc (Fig. 10a). Hence, backarc spreading, arc-continent collision and extension-induced magmatism and exhumation (Fig. 8d, e) can coevally occur in different segments of one tectonic system.

The Solomon Islands – Papua New Guinea region of the southwest Pacific has undergone two separate subduction reversals related to the collisions with the Ontong Java Plateau (Mann and Taira, 2004; Taira et al., 2004) and the Australian margin (Abers and McCaffrey, 1994). These are two subduction reversals that are analogous to elements of both the singular and composite terrane model where YTTc could have collided with an outboard tectonic fragment leading to a Mississippian subduction reversal (Fig. 7a). Clinton Creek and Midnight Dome ophiolite complexes, along with other middle Permian ophiolites (e.g. Parsons et al., 2018a) formed in the upper plate and may be analogous to ophiolites that are forming in the Bismarck Sea coeval with the ongoing collision of the New Britain Arc with the Australian margin in the Finisterre Range of the Huon Peninsula. The Australian margin is partly subducted under the New Britain Arc during the collision and provides another potential mechanism for juxtaposition of two distinct, non-synchronous eclogite belts in the YTT, an early Mississippian eclogite (Erdmer et al., 1998; Devine et al., 2006) that could have formed in the arc-trench gap of the oceanic YTTj and middle Permian eclogite (e.g. Petrie et al., 2015) that formed part of the subducting continental YTTc (Fig. 8b).

The Australian margin is subducted beneath the New Britain Arc and is likely subjected to eclogite-facies metamorphism at the same time as it is extending in the Woodlark Basin further to the east. The geological relationships provide two distinctly different analogues for emplacement of orogenic peridotites and eclogite facies metamorphism in the same plate. This is a conservative scenario to explain the complicated relationships in the composite YTT, but requires that continental YTTc is on the subducting plate (Figs. 8a, 9). However, this region also serves as another cautionary note for two reasons: (i) calc-alkaline magmatism in the Woodlark rift is not related to subduction even though it is coeval with the active segments of the New Britain-Solomon Islands arc system (Fig. 10a, b). Rather this magmatism is related to continental rifting and melting of previously subduction-modified mantle (Stolz et al., 1993). (ii) Eclogite is exhumed in the D'Entrecasteaux region, close to the western tip of the Woodlark Basin, but this eclogite is not associated with any active subduction zone. Rather it is related to exhumation of the deeper parts of a Miocene orogen, which formed between the rifted Australian margin and an outboard island arc terrane (Webb et al., 2014). If the Papuan Peninsula and Woodlark Basin area are indeed a viable analogue to the continental YTTc, it would imply that the continental Klondike “Arc” magmatism might actually represent a continental extensional province (e.g. Parsons et al., 2018a, 2018b) that is coeval with orogenic peridotite exhumation on the same plate that was subducted along strike beneath the oceanic YTTj. In this scenario, Permian eclogites provide a constraint on the age of the collision (Fig. 8b) only if they formed in the position similar to the subducted Australian margin in the Finistere Range.

7.4. Pre-Permian postulations

The composite YTT hypothesis presented above (Fig. 8) improves the singular terrane based tectonic models (Fig. 7) and has a modern analogue in oceanic arc-continent collisions (e.g. Fig. 10a). However, this hypothesis (Parsons et al., 2018a) has difficulties providing a viable tectonic model for the pre-Permian evolution in the current tectonic framework. Specifically, this model is inconsistent with the inferred Late Devonian-early Mississippian opening of the SMO in previous models (e.g Colpron et al., 2007) and the required onset of east-directed subduction in SMO to generate the early Mississippian eclogite (Fig. 8a, b). It is highly unlikely that enough oceanic lithosphere was formed in

the SMO by spreading within these time constraints to sustain subduction for over 90 my.

The composite YTT hypothesis and the modern analogues in the Australian and Pacific plate boundary zone discussed above provide an alternative model with respect to the polarity of subduction, formation of an oceanic arc-backarc terrane and opening the SMO. Most models (e.g. Nelson, 1993) assume that the present distribution of terranes is more or less indicative of their original paleogeographic position relative to each other and to the Laurentian margin (SMT mainly situated immediately east of YTT, hence formed between it and Laurentia). These models focus on the accretionary history, but they commonly ignore post-collisional extension in their 'palinspastic' reconstructions. Specifically, large portions of the YTTc are now known to have undergone exhumation in the Early Jurassic and later (e.g., Currie and Parrish, 1993; Berman et al., 2007; Knight et al., 2013; Staples et al., 2016; Morneau, 2017; Shirmohammad et al., 2011; Joyce et al., 2015). Jurassic and later exhumation of the YTTc indicates that the present distribution of terranes is not necessarily indicative of their relative paleogeographic position, but rather is a configuration that was established long after the closure of the SMO. Hence, the present distribution of terranes, with YTTc exhumed predominantly to the west of the YTTj, is an artefact of Mesozoic structural evolution and erosion and not necessarily indicative of the Paleozoic subduction polarity.

The simplest way of explaining the apparent longevity of Paleozoic subduction is by considering that YTTj originated outboard in Panthalassa above a west-dipping subduction zone (Fig. 9a). In this model, YTTj did not originate in a narrow SMO backarc seaway to the east of YTTc, but represents a part of a suprasubduction zone oceanic terrane situated west of YTTc in Panthalassa. The Late Devonian – earliest Mississippian rift-related magmatism in Laurentia and YTTc would be akin to magmatism along the eastern Australian margin (Fig. 10b), which culminated in the Mesozoic to Tertiary separation of Lord Howe Rise and Norfolk Ridge (Schellart et al., 2006). The processes discussed in Fig. 8 to explain the nearly coeval obduction of the YTTj and exhumation of orogenic peridotite apply to this model as well, because both models create a similar geometry with YTTj structurally lying structurally above YTTc, followed by west-directed subduction in SMO (Fig. 9b, c). This model implies that a large part of the SMT rocks did not originate in the SMO as proposed by Nelson (1993) and Colpron and Nelson (2009), but outboard in the Panthalassa Ocean. To avoid confusion, we kept the SMO in Figs. 7, 8 and 9 as the ocean basin that was opening behind YTTc while it was moving westwards after rifting from Laurentia. However, we propose that the term SMO should be abandoned to avoid confusion with the proposed location where a large portion of the SMT (YTTj) was formed and instead replaced by Angayucham Ocean (cf. Colpron and Nelson, 2009; Sigloch and Mihalynuk, 2017). Nevertheless, it is possible that some ocean floor rocks of the oceanic seaway (SMO/Angayucham Ocean) that separated composite YTT from Laurentia were incorporated into the SMT during its terminal Mesozoic closure (Parsons et al., 2018a).

Formation of YTTj outboard in Panthalassa is attractive, because it could also explain the spatial association of continental rifting-related volcanic rocks (Fire Lake Formation) with boninites in the Finlayson district (Murphy et al., 2006, Fig. 6; Ryan et al., 2017). Rift-related volcanic rocks may have formed in a setting similar to the northern Norfolk Ridge (Fig. 10a, b), whereas the boninites originated in a setting such as the southern New Hebrides island arc (Monzier et al., 1993). Norfolk Ridge and New Hebrides island arc are going to collide in the near future (Fig. 10a), coeval with the ongoing collision between the on-strike New Britain island arc and the Australian margin. In addition, slab-pull of the segment of Panthalassa Ocean attached to YTTc subducting westwards beneath YTTj potentially could have moved YTTc a large distance from Laurentia after it had separated from it, opening a significantly wide oceanic basin behind it by spreading. This oceanic basin equates with the SMO and the along strike Angayucham Ocean further to the north of Nelson (1993) and Colpron and Nelson (2009). Following the middle Permian-early Triassic Klondike collision between the oceanic arc-backarc terrane (YTTj or the Dunite Peak oceanic arc of Parsons et al. (2018a) and YTTc, subduction would have stepped back in the trailing Slide Mountain/Angayucham Ocean, the closure of which is probably preserved in the vertical slab wall imaged by tomography in the mantle beneath North America (Sigloch and Mihalynuk, 2013, 2017; Hildebrand, 2014). The time span of accretion of composite YTT to Laurentia and its possible complex interactions with other Mesozoic terranes (e.g. Stikinia-Quesnellia) forming an even larger composite terrane (Johnston, 2008; Hildebrand, 2013), prior to its Jurassic-Cretaceous arrival at the Laurentian margin (e.g. Evenchick et al., 2007; Pană and van der Pluijm, 2015; Sigloch and Mihalynuk, 2017), is still a matter of debate and outside the scope of this paper.

8. Conclusions

Investigation of the Clinton Creek and Midnight Dome ophiolite complexes revealed that they formed in a suprasubduction zone spreading centre at ca. 265 Ma and were subsequently rapidly tectonically emplaced onto the YTTc during the Klondike orogeny as proposed by Parsons et al. (2018a) for other Permian ophiolite complexes obducted onto YTTc and correlative SSZ volcanic rocks in the SMT. The Permian age of the SSZ setting and tectonic position above the YTTc indicate that these ophiolites did not form part of the subducting SMO floor during the Permian and that parts of the SMT have been erroneously assigned to the subducting plate in previous tectonic models. Formation of middle Permian SSZ ophiolite complexes, obduction rather than subduction of ophiolite complexes, juxtaposition of Mississippian and Permian eclogites along the suture between YTT and Laurentia (e.g., Erdmer et al., 1998; Devine et al., 2006), and broadly coeval exhumation of orogenic peridotites (e.g., Canil et al., 2003; Johnston et al., 2007) are difficult to reconcile with existing tectonic models. These relationships require YTT to be composite and composed of an oceanic arc-backarc terrane (YTTj) obducted onto a continental fragment (YTTc) outboard of Laurentia. This composite terrane was subsequently emplaced onto Laurentia during the Jurassic-Cretaceous.

Although the Sea of Japan has been used to explain the evolution of the SMO (e.g., Creaser et al., 1997a, 1999), comparison of the observed relationships to modern analogues in the Australia-Pacific boundary zone combined with the time constraints on rifting and opening of the SMO, provides a viable alternative. In this alternative, the SMO (Angayucham Ocean) formed during rifting of YTTc from the Laurentian margin but did not host Permian subduction (Fig. 9). The Laurentian margin and YTTc are represented by Australia and outboard continental ribbon(s) (Lord Howe and Norfolk ridges), respectively, whereas YTTj is represented by parts of the New Britain-Solomon-New Hebrides arc (Fig. 10b) and respective back-arc spreading centres, including production of boninite (Monzier et al., 1993). In this alternative model, YTTj originated outboard in the Panthalassa Ocean rather than in the probably narrow SMO seaway. In addition, several diachronous collisions, arc and rifting episodes that are ongoing in the Australia-Pacific boundary region (e.g., Hall, 2002; Baldwin et al., 2012; Webb et al., 2014) could explain the disparate Carboniferous-Permian tectonic, metamorphic and magmatic events and unconformities recognised in the YTT (Colpron et al., 2006a, 2007; Berman et al., 2007). The tectonic mechanisms responsible for YTTc's rifting and drifting away from Laurentia as well the subsequent Mississippian initiation of west-directed subduction outboard in Panthalassa are not well understood, but Late Devonian deformation, metamorphism and coeval magmatism in YTTc (see section of YTT as a singular terrane) hints at an important tectonic event that may be related to these processes.

Acknowledgements

The authors are grateful to members of the British Columbia (JoAnne Nelson, Mitch Mihalynuk) and Yukon geological surveys

(Maurice Colpron and Don Murphy) for their introduction into the complex Paleozoic and Mesozoic geology of the Intermontane Belt of the Canadian Cordillera, sharing data as well logistical support. The first (CvS) and third author (WMcL) would like to acknowledge close cooperation with Jane Gilotti and Meredith Petrie on the geology of the St. Cyr klippe. Detailed and careful journal reviews by Tekla Harms and Dan Gibson were very useful and improved the paper. The first author (CvS) would also like to thank Brendan, Alex and Shoufa for organizing this special volume. This is NRCan contribution #20180125.

References

Abbott, G., 1983. Origin of the Clinton Creek Asbestos Deposit. Yukon Exploration and Geology 1982: Exploration and Geological Services Division, Yukon, Indian and Northern Affairs Canadapp. 18–25.
Abbott, L.D., Silver, E.A., Galewsky, J., 1994. Structural evolution of a modern arc-continent collision in Papua New Guinea. Tectonics 13 (5), 1007–1034.
Abers, G.A., McCaffrey, R., 1994. Active arc-continent collision; earthquakes, gravity anomalies, and fault kinematics in the Huon-Finisterre collision zone, Papua New Guinea. Tectonics 13 (2), 227–245.
Anders, E., Grevesse, N., 1989. Abundances of the elements; meteoritic and solar. Geochim. Cosmochim. Acta 53 (1), 197–214.
Anonymous, 1972. Penrose field conference on ophiolites. Geotimes 17 (12), 22–24.
Baldwin, S.L., Fitzgerald, P.G., Webb, L.E., 2012. Tectonics of the New Guinea region. Annu. Rev. Earth Planet. Sci. 40, 495–520.
Barth, A.P., Wooden, J.L., 2006. Timing of magmatism following initial convergence at a passive margin, Southwestern U.S. Cordillera, and ages of lower crustal magma sources. J. Geol. 114 (2), 231–245.
Barth, A.P., Wooden, J.L., 2010. Coupled elemental and isotopic analyses of polygenetic zircons from granitic rocks by ion microprobe, with implications for melt evolution and the sources of granitic magmas. Chem. Geol. 277 (1–2), 149–159.
Bedard, J.H., Escayola, M., 2010. The advocate ophiolite mantle, Baie Verte, Newfoundland; regional correlations and evidence for metasomatism. Can. J. Earth Sci. 47 (3), 17.
Belasky, P., Stevens, C.H., Hanger, R.A., 2002. Early Permian location of western North American terranes based on brachiopod, fusulinid, and coral biogeography. Palaeogeogr. Palaeoclimatol. Palaeoecol. 179 (3–4), 245–266.
Belasky, P., Haggart, J.W., Stevens, C.H., Enkin, R.J., Monger, J.W.H., 2006. Permian faunas of westernmost North America; paleobiogeographic constraints on Permian positions of Cordilleran terranes. In: Haggart, J.W., Enkin, R.J., Monger, J.W.H. (Eds.), Paleogeography of the North American Cordillera: Evidence for and Against Large-scale Displacements. 46. Geological Association of Canada, pp. 71–80.
Beranek, L.P., Mortensen, J.K., 2011. The timing and provenance record of the Late Permian Klondike Orogeny in northwestern Canada and arc-continent collision along western North America. Tectonics 30 (5).
Berman, R.G., Ryan, J.J., Gordey, S.P., Villeneuve, M., 2007. Permian to Cretaceous polymetamorphic evolution of the Stewart River region, Yukon-Tanana Terrane, Yukon, Canada; P-T evolution linked with in situ SHRIMP monazite geochronology. J. Metamorph. Geol. 25 (7), 803–827.
Black, L.P., Kamo, S.L., Allen, C.M., Davis, D.W., Aleinikoff, J.N., Valley, J.W., Mundil, R., Campbell, I.H., Korsch, R.J., Williams, I.S., Foudoulis, C., 2004. Improved $^{206}Pb^{238}U$ microprobe geochronology by the monitoring of a trace-element-related matrix effect; SHRIMP, ID-TIMS, ELA-ICP-MS and oxygen isotope documentation for a series of zircon standards. Chem. Geol. 205 (1–2), 115–140.
Breitsprecher, K., Mortensen, J.K., 2004. Yukon Age 2004 - A Database of Isotopic Age Determinations for Rock Units in Yukon Territory. Yukon Geological Survey, CD-ROM.
Brown, D., Ryan, P.D., Afonso, J.C., Boutelier, D., Burg, J.P., Byrne, T., Calvert, A., Cook, F., Debari, S., Dewey, J.F., Gerya, T.V., Harris, R., Herrington, R., Konstantinovskaya, E., Reston, T., Zagorevski, A., 2011. Arc–continent collision: the making of an orogen. In: Brown, D., Ryan, P.D. (Eds.), Arc-Continent Collision. Springer Berlin Heidelberg, Berlin, Heidelberg, pp. 477–493.
Cabanis, B., Lecolle, M., 1989. Le diagramme La/10-Y/15-Nb/8; un outil pour la discrimination des series volcaniques et la mise en evidence des processus de melange et/ou de contamination crustale. The La/10-Y/15-Nb/8 diagram; a tool for distinguishing volcanic series and discovering crustal mixing and/or contamination: Comptes Rendus de l'Academie des Sciences, Serie 2, Mecanique, Physique, Chimie, Sciences de l'Univers. Sci. Terre 309 (20), 2023–2029.
Calvert, A.J., 1996. Seismic reflection constraints on imbrication and underplating of the northern Cascadia convergent margin. Can. J. Earth Sci. 33 (9), 1294–1307.
Canil, D., Johnston, S.T., 2003. Harzburgite Peak: a large mantle tectonite massif in ophiolite from southwest Yukon. In: Emond, D.S., Lewis, L.L. (Eds.), 2002 Yukon Exploration and Geology Exploration and Geological Services Division, Yukon Region. Indian and Northern Affairs Canada, pp. 77–84.
Canil, D., Johnston, S.T., Evers, K., Shellnutt, J.G., Creaser, R.A., 2003. Mantle exhumation in an early Paleozoic passive margin, northern Cordillera, Yukon. J. Geol. 111 (3), 313–327.
Cloos, M., 1993. Lithospheric buoyancy and collisional orogenesis; subduction of oceanic plateaus, continental margins, island arcs, spreading ridges, and seamounts. Geol. Soc. Am. Bull. 105 (6), 715–737.
Colpron, M., Nelson, J.L., 2009. A Paleozoic Northwest Passage: incursion of Caledonian, Baltican and Siberian terranes into eastern Panthalassa and the early evolution of the North American Cordillera. In: Cawood, P.A., Kroner, A. (Eds.), Earth Accretionary Systems in Space and Time. 318. The Geological Society, London, Special Publications, pp. 273–307.
Colpron, M., Nelson, J.L., 2011. A Digital Atlas of Terranes for the Northern Cordillera. BC GeoFile 2011-11.
Colpron, M., Gladwin, K., Johnston, S.T., Mortensen, J.K., Gehrels, G.E., 2005. Geology and juxtaposition history of the Yukon-Tanana, Slide Mountain, and Cassiar Terranes in the Glenlyon area of central Yukon. Can. J. Earth Sci. 42 (8), 1431–1448.
Colpron, M., Mortensen, J.K., Gehrels, G.E., Villeneuve, M., 2006a. Basement complex, Carboniferous magmatism and Paleozoic deformation in Yukon-Tanana Terrane of central Yukon; field, geochemical and geochronological constraints from Glenlyon map area. In: Colpron, M., Nelson, J.L. (Eds.), Paleozoic Evolution and Metallogeny of Pericratonic Terranes at the Ancient Pacific Margin of North America, Canadian and Alaskan Cordillera. Vol. 45. Geological Association of Canada, pp. 131–151.
Colpron, M., Nelson, J.L., Murphy, D.C., 2006b. A tectonostratigraphic framework for the pericratonic terranes of the northern Canadian Cordillera. In: Colpron, M., Nelson, J.L. (Eds.), Paleozoic Evolution and Metallogeny of Pericratonic Terranes at the Ancient Pacific Margin of North America, Canadian and Alaskan Cordillera. Vol. 45. Geological Association of Canada, pp. 1–23.
Colpron, M., Nelson, J.L., Murphy, D.C., 2007. Northern Cordilleran terranes and their interactions through time. GSA Today 17 (4–5), 4–10.
Colpron, M., Israel, S., Murphy, D., Pigage, L., Moynihan, D., 2016. Yukon Bedrock Geology Map, Yukon Geological Survey, Open File 2016-1, Scale 1:1 000 000, Map and Legend.
Colpron, M., Carr, S., Hildes, D., Piercey, S., 2017. Geophysical, geochemical and geochronological constraints on the geology and mineral potential of the Livingstone Creek area, south-central Yukon (NTS 105E/8). In: MacFarlane, K.E., Weston, L.H. (Eds.), Yukon Exploration and Geology Overview 2016. Yukon Geological Survey, pp. 47–86.
Creaser, R.A., Erdmer, P., Stevens, R.A., Grant, S.L., 1997a. Tectonic affinity of Nisutlin and Anvil assemblage strat from the Teslin tectonic zone, northern Canadian Cordillera: constraints from neodymium isotope and geochemical evidence. Tectonics 16, 107–121.
Creaser, R.A., Heaman, L.M., Erdmer, P., 1997b. Timing of high-pressure metamorphism in the Yukon – Tanana terrane, Canadian Cordillera: constraints from U – Pb zircon dating of eclogite from the Teslin tectonic zone. Can. J. Earth Sci. 34, 709–715.
Creaser, R.A., Goodwin-Bell, J.-A.S., Erdmer, P., 1999. Geochemical and Nd isotopic constraints for the origin of eclogite protoliths, northern Cordillera; implications for the Paleozoic tectonic evolution of the Yukon-Tanana Terrane. Can. J. Earth Sci. 36 (10), 1697–1709.
Currie and Parrish, 1993. Jurassic accretion of Nisling terrane along the western margin of stikinia, coast mountains, northwestern British Columbia. Geology 21, 235–238.
Davey, F.J., Granot, R., Cande, S.C., Stock, J.M., Selvans, M., Ferraccioli, F., 2016. Synchronous oceanic spreading and continental rifting in West Antarctica. Geophys. Res. Lett. 43 (12), 6162–6169.
De Keijzer, M., Williams, P.F., Carr, S.D., 2000. Reflections on Lithoprobe SNORCLE Line 31 in light of the structure of the Teslin zone in the Last Peak area (NTS map 105 E/9), southern Yukon Territory. In: Cook, F., Erdmer, P. (Eds.), Slave – North American Cordillera Lithospheric Evolution (SNORCLE) Transect and Cordilleran Tectonics Workshop Meeting. 72. Lithoprobe Report, Calgary, Alberta, pp. 114–118.
Devine, F., Colpron, M., Carr, S.D., Murphy, D.C., Davis, W.J., Smith, S., Villeneuve, M., Nelson, J.L., 2006. Geochronological and geochemical constraints on the origin of the Klatsa metamorphic complex; implications for early Mississippian high-pressure metamorphism within Yukon-Tanana Terrane. In: Colpron, M., Nelson, J.L. (Eds.), Paleozoic Evolution and Metallogeny of Pericratonic Terranes at the Ancient Pacific Margin of North America, Canadian and Alaskan Cordillera. Vol. 45. Geological Association of Canada, pp. 107–130.
Dick, H.J.B., Bullen, T., 1984. Chromian spinel as a petrogenetic indicator in abyssal and alpine-type peridotites and spatially associated lavas. Contrib. Mineral. Petrol. 86 (1), 54–76.
Dusel-Bacon, C., Colpron, M., Hopkins, M.J., Mortensen, J.K., Dashevsky, S.S., Bressler, J.R., Day, W.C., Nelson, J.L., 2006. Paleozoic tectonic and metallogenic evolution of the pericratonic rocks of east-central Alaska and adjacent Yukon. In: Colpron, M., Nelson, J.L. (Eds.), Paleozoic Evolution and Metallogeny of Pericratonic Terranes at the Ancient Pacific Margin of North America, Canadian and Alaskan Cordillera. Vol. 45. Geological Association of Canada, pp. 25–74.
Dusel-Bacon, C., Day, W.C., Aleinikoff, J.N., 2013. Geochemistry, petrography, and zircon U-Pb geochronology of Paleozoic metaigneous rocks in the Mount Veta area of east-central Alaska; implications for the evolution of the westernmost part of the Yukon-Tanana Terrane. Can. J. Earth Sci. 50 (8), 826–846.
Erdmer, P., Armstrong, R.L., 1988. Permo-Triassic isotopic dates for Blueschist, Ross River Area, Yukon. In: Abbott, J.G. (Ed.), Yukon Geology. Vol. 2. Indian & Northern Affairs Canada, Exploration & Geological Services Division, Yukon, pp. 33–36.
Erdmer, P., Helmstaedt, H., 1983. Eclogite from central Yukon; a record of subduction at the western margin of ancient North America. Can. J. Earth Sci. 20 (9), 1389–1408.
Erdmer, P., Ghent, E.D., Archibald, D.A., Stout, M.Z., 1998. Paleozoic and Mesozoic high-pressure metamorphism at the margin of ancestral North America in central Yukon. GSA Bull. 110, 615–629.
Evenchick, C.A., McMechan, M.E., McNicoll, J., Carr, S.D., 2007. A synthesis of the Jurassic-Cretaceous tectonic evolution of the central and southwestern Canadian cordillera: exploring links across the orogen. In: Sears, J.W., Harms, T.A., Evenchick, C.A. (Eds.), Whence the Mountains? Inquiries Into the Evolution of Orogenic Systems: A Volume in Honor of Raymond A. Price. 433. Geological Society of America Special Paper, pp. 117–145.
Fallas, K.M., Cook, F., Erdmer, P., Archibald, D.A., Heaman, L.M., Creaser, R.A., Erdmer, P., 1998. The St. Cyr Klippe, south-central Yukon; an outlier of the Teslin tectonic

zone? In: Lithoprobe Report, pp. 131–138.
Foster, H.L., Keith, T.E.C., 1974. Ultramafic rocks of the Eagle Quadrangle, east-central Alaska. J. Res. U. S. Geol. Surv. 2 (6), 657–669.
Foster, H.L., Keith, T.E.C., Menzie, W.D., 1994. Geology of the Yukon-Tanana area of east-central Alaska. In: Plafker, G., Berg, H.C. (Eds.), The Geology of Alaska. Geological Society of America, pp. 205–240.
Gabrielse, H., Mortensen, J.K., Parrish, R.R., Harms, T.A., Nelson, J.L., van der Heyden, P., 1993. Late Paleozoic Plutons in the Sylvester Allochthon, North-central British Columbia: Radiogenic Age and Isotopic Studies: Report 7. 93-2. Geological Survey of Canada, Paper, pp. 107–118.
Gabrielse, H., Murphy, D.C., Mortensen, J.K., 2006. Cretaceous and Cenozoic dextral orogen-parallel displacements, magmatism and paleogeography, north-central Canadian Cordillera. In: Haggart, J.W., Enkin, R.J., Monger, J.W.H. (Eds.), Paleogeography of the North American Cordillera: Evidence for and Against Large-scale Displacements. Vol. 46. Geological Association of Canada, Special Paper, pp. 255–276.
Galewsky, J., Silver, E.A., Gallup, C.D., Edwards, R.L., Potts, D.C., 1996. Foredeep tectonics and carbonate platform dynamics in the Huon Gulf, Papua New Guinea. Geology 24 (9), 819–822.
Gehrels, G.E., McClelland, W.C., Samson, S.D., Patchett, P.J., Orchard, M.J., 1992. Geology of the western flank of the Coast Mountains between Cape Fanshaw and Taku Inlet, southeasternAlaska. Tectonics 11 (3), 567–585. https://doi.org/10.1029/92TC00482.
Gilotti, J.A., McClelland, W.C., van Staal, C.R., Petrie, M.B., 2017. Detrital zircon evidence for eclogite formation by basal subduction erosion – an example from the Yukon-Tanana composite arc, Canadian Cordillera. Geol. Soc. Am. Spec. Pap. 526 (17 p).
Goodwin-Bell, J.-A., 1998. A Geochemical and Sm-Nd Isotopic Study of Cordilleran Eclogites From the Yukon-Tanana Terrane. MSc Thesis. University of Alberta, Edmonton, AB, pp. 145.
Gordey, S.P., 2002. Is Yukon-Tanana Terrane North America? In: Cook, F., Erdmer, P. (Eds.), SNORCLE Transect and Cordilleran Tectonics Workshop Meeting. Pacific Geoscience Centre. Lithoprobe Report. 82. pp. 39–42.
Gordey, S.P., Geldsetzer, H.H.J., Morrow, D.W., Bamber, E.W., Henderson, C.W., Richards, B.C., 1991. Upper Devonian to Middle Jurassic assemblages. Part A, Ancestral North America. In: Gabrielse, H., Yorath, C. (Eds.), Geology of the Cordilleran Orogen in Canada. G2. Geological Society of America Decade of North American Geology, pp. 221–328.
Hall, R., 2002. Cenozoic geological and plate tectonic evolution of SE Asia and the SW Pacific: computer-based reconstructions, model and animations. J. Asian Earth Sci. 20 (4), 353–431.
Harms, T.A., Murchey, B.L., 1992. Setting and occurrence of late Paleozoic radiolarians in the Sylvester Allochthon, part of a proto-Pacific ocean floor terrane in the Canadian Cordillera. Palaeogeogr. Palaeoclimatol. Palaeoecol. 96 (1–2), 127–139.
Hildebrand, R.S., 2013. Mesozoic Assembly of the North American Cordillera. 495 GSA Special Paper 169p.
Hildebrand, R.S., 2014. Geology, Mantle tomography, and inclination corrected paleogeographic trajectories support westward subduction during Cretaceous orogenesis in the north american Cordillera. In: Hibbard, J.P., Pollock, J.C., Murphy, J.B., van Staal, C.R., Greenough, J.D. (Eds.), Reeltime Geological Syntheses -Remembering Harold 'Hank' Williams. 10. Geoscience Canada Reprint Series, pp. 439–456.
Htoon, M., 1981. Isotopic age determinations of some metamorphic and igneous rocks from Clinton Creek area, Yukon. In: Tempelman-Kluit, D.J. (Ed.), Yukon Geology and Exploration 1979–80. Indian and Northern Affairs Canada, Exploration & Geological Services Division, pp. 65–67.
Huang, C., Yuan, P., Tsao, S., 2006. Teporal and spatial record of active arc-continent collision in Taiwan: a synthesis. Geol. Soc. Am. Bull. 118, 274–288.
von Huene, R., Scholl, D.W., 1991. Observations at convergent margins concerning sediment subduction, subduction erosion, and the growth of continental crust. Rev. Geophys. 29 (3), 279–316.
Jagoutz, O., Müntener, O., Manatschal, G., Rubatto, D., Péron-Pinvidic, G., Turrin, B.D., Villa, I.M., 2007. The rift-to-drift transition in the North Atlantic: a stuttering start of the MORB machine? Geology 35, 1087–1090.
Johnston, S.T., 2008. The cordilleran ribbon continent of North America. Annu. Rev. Earth Planet. Sci. 36, 495–530.
Johnston, S.T., Canil, D., Heaman, L.H., 2007. Permian exhumation of the Buffalo Pitts orogenic peridotite massif, northern Cordillera, Yukon. Can. J. Earth Sci. 44 (3), 275–286.
Joyce, N.L., Ryan, J.J., Colpron, M., Hart, C.J.R., Murphy, D.C., 2015. A compilation of $^{40}Ar/^{39}Ar$ age determinations for igneous and metamorphic rocks, and mineral occurrences from central and southeast Yukon. Pap. Geol. Surv. Can. 7924, 229.
Kimura, G., Ludden, J., 1995. Peeling oceanic crust in subduction zones. Geology 23 (3), 217–220.
Knight, E., Schneider, D.A., Ryan, J.J., 2013. Thermochronology of the Yukon-Tanana Terrane, West-Central Yukon: evidence for Jurassic extension and exhumation in the Northern Canadian Cordillera. J. Geol. 121, 371–400.
Korotev, R.L., 1996. On the relationship between the Apollo 16 ancient regolith breccias and feldspathic fragmental breccias, and the composition of the prebasin crust in the Central Highlands of the Moon. Meteoritics 31 (3), 403–412.
Lallemand, S., Heuret, A., Boutelier, D., 2005. On the relationships between slab dip, back-arc stress, upper plate absolute motion, and crustal nature in subduction zones. Geochm. Geophys. Geosyst. 18.
Little, T.A., Hacker, B.R., Gordon, S.M., Baldwin, S.L., Fitzgerald, P.G., Ellis, S., Korchinski, M., 2011. Diapiric exhumation of Earth's youngest (UHP) eclogites in the gneiss domes of the D'Entrecasteaux Islands, Paepua New Guinea. Tectonophysics 510 (1–2), 39–68.
Ludwig, K.R., 2003. User's Manual for Isoplot/Ex re3.00: A Geochronological Toolkit for Microsoft Excel. 4 Berkeley Geochronology Center, Berkeley Special Publication. (70 p).
MacLeod, C.J., Searle, R.C., Murton, B.J., Casey, J.F., Mallows, C., Unsworth, S.C., Achenbach, K.L., Harris, M., 2009. Life cycle of oceanic core complexes. Earth Planet. Sci. Lett. 287 (3–4), 333–344.
Manatschal, G., 2004. New models for evolutionof magma-poor rifted marginsbased on a review of data and concepts from West Iberia and the Alps. Int. J. Earth Sci. 93, 432–466.
Manatschal, G., Engstrom, A., Desmurs, L., Schaltegger, U., Cosca, M., Muntener, O., Bernoulli, D., 2006. What is the tectono-metamorphic evolution of continental break-up: the example of the Tasna Ocean-Continent transition. J. Struct. Geol. 28, 1849–1869.
Manatschal, G., Montanini, A., Sauter, D., Karpoff, A.M., Masini, E., Mohn, G., Lagabrielle, Y., Piccardo, G.B., Tribuzio, R., Dick, H.J.B., 2011. The Chenaillet Ophiolite in the French/Italian Alps; an ancient analogue for an oceanic core complex? Lithos 124 (3–4), 169–184.
Mann, P., Taira, A., 2004. Global tectonic significance of the Solomon Islands and Ontong Java Plateau convergent zone. Tectonophysics 389 (3–4), 137–190.
Mattinson, J.M., 2010. Analysis of the relative decay constants of ^{235}U and ^{238}U by multi-step CA-TIMS measurements of closed system natural zircon samples. Chem. Geol. 275 (3–4), 186–198.
McIntosh, K., Nakamura, Y., Wang, T.K., Shih, R.C., Chen, A., Liu, C.S., 2005. Crustal-scale seismic profiles across Taiwan and the western Philippine Sea. Tectonophysics 401 (1–2), 23–54.
Mihalynuk, M.G., Friedman, R.M., Devine, F., Heaman, L.M., 2006. Protolith age and deformation history of the Big salmon Complex, relicts of a Paleozoic continental arc in northern British Columbia. In: Colpron, M., Nelson, J.L. (Eds.), Paleozoic Evolution and Metallogeny of Pericratonic Terranes at the Ancient Pacific Margin of North America, Canadian and Alaskan Cordillera 45. Geological Association of Canada, pp. 179–200.
Miranda, E.A., Dilek, Y., 2010. Oceanic core complex development in modern and ancient oceanic lithosphere; gabbro-localized versus peridotite-localized detachment models. J. Geol. 118 (1), 95–109.
Mohn, G., Manatschal, G., Müntener, O., Beltrando, M., Masini, E., 2010. Unravelling the interaction between tectonic and sedimentary processes during lithospheric thinning in the Alpine Tethys margins. Int. J. Earth Sci. 99, 75–101.
Monzier, M., Danyushevsky, L.V., Crawford, A.J., Bellon, H., Cotten, J., 1993. High-Mg andesites from the southern termination of the New Hebrides island arc (SW Pacific). J. Volcanol. Geotherm. Res. 57 (3–4), 193–217.
Morneau, Y.E., 2017. Tectono-metamorphic Evolution of the Snowcap Assemblage, Yukon-Tanana Terrane, West-Central Yukon. MSc Thesis. Carleton University, Ottawa, ON, Canada, pp. 199.
Mortensen, J.K., 1990. Geology and U–Pb geochronology of the Klondike District, west-central Yukon Territory. Can. J. Earth Sci. 27, 903–914.
Mortensen, J.K., 1992. Pre-mid-Mesozoic tectonic evolution of the Yukon-Tanana Terrane, Yukon and Alaska. Tectonics 11 (4), 18.
Murphy, D.C., Colpron, M., Mortensen, J.K., Piercey, S.J., Orchard, M.J., Gehrels, G.E., Nelson, J.L., 2006. Mid-Paleozoic to early Mesozoic tectonostratigraphic evolution of Yukon-Tanana and Slide Mountain terranes and affiliated overlap assemblages, Finlayson Lake massive sulphide district, southeastern Yukon. In: Colpron, M., Nelson, J.L. (Eds.), Paleozoic Evolution and Metallogeny of Pericratonic Terranes at the Ancient Pacific Margin of North America, Canadian and Alaskan Cordillera. 45. Geological Association of Canada, pp. 75–105.
Nelson, J.L., 1993. The Sylvester Allochthon; upper Paleozoic marginal-basin and island-arc terranes in northern British Columbia. Can. J. Earth Sci. 30 (3), 631–643.
Nelson, J.L., Bradford, J.A., 1993. Geology of the Midway-Cassiar area, northern British Columbia (^{104}O, ^{104}P). Minist. Energy Min. Pet. Resour. Bull. 83, 94.
Nelson, J.L., Colpron, M., Piercey, S.J., Dusel-Bacon, C., Murphy, D.C., Roots, C.F., Nelson, J.L., 2006. Paleozoic tectonic and metallogenetic evolution of pericratonic terranes in Yukon, northern British Columbia and eastern Alaska. In: Colpron, M., Nelson, J.L. (Eds.), Paleozoic Evolution and Metallogeny of Pericratonic Terranes at the Ancient Pacific Margin of North America, Canadian and Alaskan Cordillera. 45. Geological Association of Canada, pp. 323–360.
Nelson, J.L., Colpron, M., Israel, S., 2013. In: Bissig, T., Rusk, B.G., Thompson, J.F.H. (Eds.), The Cordillera of British Columbia, Yukon, and Alaska; Tectonics and Metallogeny. 17. Special Publication [Society of Economic Geologists [U. S.]], pp. 53–109.
Niu, Y., Herzberg, C., Wilson, M., 2004. Bulk-rock major and trace element compositions of abyssal peridotites; implications for mantle melting, melt extraction and post-melting processes beneath mid-ocean ridges. J. Petrol. 45 (12), 2423–2458.
Ohara, Y., Fujioka, K., Ishii, T., Yurimoto, H., 2003. Peridotites and gabbros from the Parece Vela backarc basin; unique tectonic window in an extinct backarc spreading ridge. Geochem. Geophys. Geosyst. 4 (7), 8611.
Oliver, D.H., 1996. Structural, kinematic and thermochronologic studies of the Teslin suture zone, south-central Yukon Territory. Unpublished Ph.D thesis, southern Methodist University, Austin, Texas, 231 pp.
Orchard, M.J., 2006. Late Paleozoic and Triassic conodont faunas of Yukon and northern British Columbia and implications for the evolution of the Yukon-Tanana terrane. In: Colpron, M., Nelson, J.L. (Eds.), Paleozoic Evolution and Metallogeny of Pericratonic Terranes at the Ancient Pacific Margin of North America, Canadian and Alaskan Cordillera. 45. Geological Association of Canada, Special Paper, pp. 229–260.
Pană, D.I., van der Pluijm, B.A., 2015. Orogenic pulses in the Alberta rocky mountains: radiometric dating of major faults and comparison with the regional tectono-stratigraphic record. GSA Bull. 127, 480–502.
Parsons, A.J., Ryan, J.J., Coleman, M., van Staal, C.R., 2017. The Slide Mountain

ophiolite, Big Salmon Range, south-central Yukon: Preliminary results from fieldwork. In: MacFarlane, K.E., Weston, L.H. (Eds.), Yukon Exploration and Geology Overview 2016. Yukon Geological Survey, pp. 181–196.
Parsons, A.J., Zagorevski, A., Ryan, J.J., McClelland, W.C., van Staal, C.R., Coleman, M.C., Golding, M.L., 2018a. Petrogenesis of the dunite Peak ophiolite, south-central yukon: a new hypothesis for the late Paleozoic-early mesozoic tectonic evolution of the northern cordillera. GSA Bull. https://doi.org/10.1130/B31964.1.
Parsons, A.J., Coleman, M.J., Ryan, J.J., Joyce, N.L., Gibson, H.D., Larson, K.P., 2018b. The Yukon River Shear Zone: a complex record of mid- to upper-crustal deformation of the Yukon-Tanana terrane, NW Cordillera. Lithosphere (in press).
Pearce, J.A., 1996. A user's guide to basalt discrimination diagrams. In: Wyman, D.A. (Ed.), Trace Element Geochemistry of Volcanic Rocks: Applications for Massive Sulphide Exploration. Vol. 12. Geological Association of Canada, Short Course, pp. 79–113.
Pearce, J.A., 2014. Immobile element fingerprinting of ophiolites. Elements 10 (2), 101–108.
Pecha, M.E., Gehrels, G.E., McClelland, W.C., Giesler, D., White, C., Yokelson, I., 2016. Detrital Zircon U-Pb geochronology and Hf- isotope geochemistry of the Yukon-Tanana terrane, Coast Mountains, southeast Alaska. Geosphere 12 (5) 19p. https://doi.org/10.1130/GES01303.1.
Perfit, M.R., Taylor, B., Langmuir, C.H., Baekisapa, M., Chappell, B.W., Johnson, R.W., Staudigel, H., Taylor, S.R., Exon, N.F., 1987. Geochemistry and petrology of volcanic rocks from the Woodlark Basin; addressing questions of ridge subduction. Earth Sci. Ser. 7, 113–154.
Petrie, M.B., Gilotti, J.A., McClelland, W.C., van Staal, C.R., Isard, S.J., 2015. Geologic setting of Eclogite-facies assemblages in the St. Cyr klippe, Yukon-Tanana terrane, Yukon, Canada. Geosci. Can. 42, 327–350.
Petrie, M.B., Massonne, H.-J., Gilotti, J.A., McClelland, W.C., Van Staal, C., 2016. The P-T path of eclogites in the St. Cyr Klippe, Yukon, Canada; Permian metamorphism of a coherent high-pressure unit in an accreted terrane of the North American Cordillera. Eur. J. Mineral. 28, 1111–1130.
Philippot, P., Blichert-Toft, J., Perchuk, A., Costa, S., Gerasimov, 2001. Lu–Hf and Ar–Ar chronometry supports extreme rate of subduction zone metamorphism deduced from geospeedometry. Tectonophysics 342, 23–38.
Piercey, S.J., Colpron, M., 2009. Composition and provenance of the Snowcap assemblage, basement to the Yukon-Tanana Terrane, northern Cordillera; implications for Cordilleran crustal growth. Geosphere 5 (5), 439–464.
Piercey, S.J., Murphy, D.C., Mortensen, J.K., Paradis, S., 2001. Boninitic magmatism in a continental margin setting, Yukon-Tanana Terrane, southeastern Yukon, Canada. Geology 29 (8), 731–734.
Piercey, S.J., Mortensen, J.K., Creaser, R.A., 2003. Neodymium isotope geochemistry of felsic volcanic and intrusive rocks from the Yukon-Tanana Terrane in the Finlayson Lake region, Yukon, Canada. Can. J. Earth Sci. 40 (1), 77–97.
Piercey, S.J., Murphy, D.C., Mortensen, J.K., Creaser, R.A., 2004. Mid-Paleozoic initiation of the northern Cordilleran marginal backarc basin; geologic, geochemical, and neodymium isotope evidence from the oldest mafic magmatic rocks in the Yukon-Tanana Terrane, Finlayson Lake District, southeast Yukon, C. Geol. Soc. Am. Bull. 116 (9–10), 1087–1106.
Piercey, S.J., Colpron, M., Nelson, J.L., Colpron, M., Dusel-Bacon, C., Simard, R.-L., Roots, C.F., Nelson, J.L., 2006. Paleozoic magmatism and crustal recycling along the ancient Pacific margin of North America, northern Cordillera. In: Colpron, M., Nelson, J.L. (Eds.), Paleozoic Evolution and Metallogeny of Pericratonic Terranes at the Ancient Pacific Margin of North America, Canadian and Alaskan Cordillera. 45. Geological Association of Canada, pp. 281–322.
Piercey, S.J., Murphy, D.C., Creaser, R.A., 2012. Lithosphere-asthenosphere mixing in a transform-dominated late Paleozoic backarc basin: implications for northern Cordilleran crustal growth and assembly. Geosphere 8, 716–739.
Plint, H.E., Gordon, T.M., 1997. The Slide Mountain Terrane and the structural evolution of the Finlayson Lake fault zone, southeastern Yukon. Can. J. Earth Sci. 34 (2), 105–126.
Pubellier, M., Bader, A.G., Rangin, C., Deffontaines, B., Quebral, R., 1999. Upper plate deformation induced by subduction of a volcanic arc; the Snellius Plateau (Molucca Sea, Indonesia and Mindanao, Philippines). Tectonophysics 304 (4), 345–368.
Reston, T., Manatschal, G., 2011. Rifted margins: building blocks of later collisions. Chapter 1. In: Brown, D., Ryan, P.D. (Eds.), Arc-Continent Collision, Frontiers in Earth Sciences.
Richards, D.R., Butler, R.F., Harms, T.A., 1993. Paleomagnetism of the late Paleozoic Slide Mountain terrane, northern and central British Columbia. Can. J. Earth Sci. 30, 898–1913.
Roback, R.C., Sevigny, J.H., Walker, N.W., 1994. Tectonic setting of the Slide Mountain Terrane, southern British Columbia. Tectonics 13 (5), 1242–1258.
Robertson, A.H.F., 2007. Evidence of continental breakup from the Newfoundland rifted margin (Ocean Drilling Program Leg 210): Lower Cretaceous seafloor formed by exhumation of subcontinental mantle lithosphere, and the transition to seafloor spreading. In: Tucholke, B.E., Sibuet, J.-C., Klaus, A. (Eds.), Proceedings of the Ocean Drilling Program, Scientific Results, vol. 210. (Ocean Drilling Program), College Station, TX, pp. 1–69.
Robinson, P.T., Malpas, J., Dilek, Y., Zhou, M., 2008. The significance of sheeted dike complexes in ophiolites. GSA Today 18 (11), 4–11.
Roots, C.F., Harms, T.A., Simard, R.-L., Orchard, M.J., Heaman, L., 2002. Constraints on the age of the Klinkit assemblage east of Teslin Lake, northern British Columbia. Bull. Geol. Surv. Can. A7, 11.
Roots, C.F., Nelson, J.L., Simard, R.L., Harms, T.A., 2006. Continental fragments, mid-Paleozoic arcs and overlapping late Paleozoic arc and Triassic sedimentation in the Yukon-Tanana terrane of northern British Columbia and southern Yukon. In: Colpron, M., Nelson, J.L. (Eds.), Paleozoic Evolution and Metallogeny of Pericratonic Terranes at the Ancient Pacific Margin of North America, Canadian and Alaskan Cordillera. 45. Geological Association of Canada, pp. 153–178.
Ross, C.A., 1969. Upper Paleozoic Fusulinacea Eowaeringella and Wedekindelina from Yukon territory and giant Parafusulina from British Columbia. Contributions to Canadian Paleontology. Bull. Geol. Surv. Can. 182.
Ruks, T.W., Piercey, S.J., Ryan, J.J., Villeneuve, M.E., Creaser, R.A., 2006. Mid- to late Paleozoic K-feldspar augen granitoids of the Yukon-Tanana Terrane, Yukon, Canada; implications for crustal growth and tectonic evolution of the northern Cordillera. Geol. Soc. Am. Bull. 118 (9–10), 1212–1231.
Ryan, J.J., Zagorevski, A., Williams, S.P., Roots, C., Ciolkiewicz, W., Hayward, N., Chapman, J.B., 2013a. Geology, Stevenson Ridge (Northeast Part), Yukon; Geological Survey of Canada, Canadian Geoscience Map 116 (2nd Edition, Preliminary), Scale 1:100 000. https://doi.org/10.4095/292407.
Ryan, J.J., Zagorevski, A., Williams, S.P., Roots, C., Ciolkiewicz, W., Hayward, N., Chapman, J.B., 2013b. Geology, Stevenson Ridge (Northwest Part), Yukon; Geological Survey of Canada, Canadian Geoscience Map 117 (2nd Edition, Preliminary), Scale 1:100 000. https://doi.org/10.4095/292408.
Ryan, J.J., Zagorevski, A., Roots, C.F., Joyce, N., 2014. Paleozoic tectonostratigraphy of the northern Stevenson Ridge area, Yukon. Bull. Geol. Surv. Can 13 p. https://doi.org/10.4095/293924.
Ryan, J.J., Nelson, J., van Staal, C.R., 2015. Fieldwork in Sylvester Allochthon, Cassiar Mountains, British Caledonides: Investigations of the Rapid River Tectonite and the Slide Mountain Terrane. Geological Fieldwork 2014, British Columbia Ministry of Energy and Mines, British Columbia Geological Survey Paper 2015-1pp. 113–128.
Ryan, J.J., Zagorevski, A., Joyce, N.L., Staples, R.D., Jones, J.V., Gibson, H.D., 2017. Mid-Cretaceous Core Complexes in the Northern Cordillera: Exposing the Parautochthon Through a Thin Flap of Allochthonous Yukon-Tanana Terrane in Western Yukon. GSA Annual Meeting, Washington, USA.
Sajona, F.G., Maury, R.C., Pubellier, M., Leterrier, J., Bellon, H., Cotten, J., 2000. Magmatic source enrichment by slab-derived melts in a young post-collision setting, central Mindanao (Philippines). Lithos 54 (3–4), 173–206.
Savov, I.P., Ryan, J.G., D'Antonio, M., Kelley, K., Mattie, P., 2005. Geochemistry of serpentinized peridotites from the Mariana forearc Conical Seamount, ODP Leg 125; implications for the elemental recycling at subduction zones. Geochem. Geophys. Geosyst. 6.
Schellart, W.P., Lister, G.S., Toy, G., 2006. A late Cretaceous and Cenozoic reconstruction of the Southwest Pacific region: Tectonics controlled by subduction and slab rollback processes. Earth Sci. Rev. 76, 191–233.
Scholl, D.W., von Huene, R., 2007. Crustal recycling at modern subduction zones applied to the past issues of growth and preservation of continental basement crust, mantle geochemistry, and supercontinent reconstruction. Mem. Geol. Soc. Am. 200, 9–32.
Schroeder, T., John, B.E., 2004. Strain localization on an oceanic detachment fault system, Atlantis Massif, 30°N, Mid-Atlantic Ridge. Geochm. Geophys. Geosyst. 5 (11), 30.
Shirmohammad, F., Wierzbowski, A., Smith, P.L., Anderson, R.G., McNicoll, J., Pienkowski, G., Sha, J., Wang, Y., 2011. The Jurassic Succession at Lisadele Lake (Tulsequah Map Area, British Columbia, Canada) and Its Bearing on the Tectonic Evolution of the Stikine Terrane. 9. Volumina Jurassica, pp. 43–60.
Sigloch, K., Mihalynuk, M.G., 2013. Intraoceanic subduction shaped the assembly of cordilleran North America. Nature 496, 50–56.
Sigloch, K., Mihalynuk, M.G., 2017. Mantle and geological evidence for a Late Jurassic–Cretaceous suture spanning North America. GSA Bull. 129, 1489–1520.
Simard, R.-L., Dostal, J., Roots, C.F., 2003. Development of late Paleozoic volcanic arcs in the Canadian Cordillera: an example from the Klinkit Group, northern British Columbia and southern Yukon. Can. J. Earth Sci. 40, 907–924.
van Staal, C.R., Dewey, J.F., MacNiocaill, C., McKerrow, S., 1998. The Cambrian-Silurian tectonic evolution of the northern Appalachians: history of a complex, southwest Pacific-type segment of Iapetus. In: Blundell, D.J., Scott, A.C. (Eds.), Lyell: The Past Is the Key to the Present. 143. Geological Society Special Publication, pp. 199–242.
van Staal, C.R., Chew, D.M., Zagorevski, A., McNicoll, V., Hibbard, J., Skulski, T., Castonguay, S., Escayola, M.P., Sylvester, P.J., 2013. Evidence of Late Ediacaran hyperextension of the Laurentian Iapetan Margin in the Birchy Complex, Baie Verte Peninsula, Northwest Newfoundland: implications for the opening of Iapetus, Formation of Peri-Laurentian Microcontinents and Taconic – Grampian Orogenesis. Geosci. Can. 40, 94–117.
Stacey, J.S., Kramers, J.D., 1975. Approximation of terrestrial lead isotope evolution by a two-stage model. Earth Planet. Sci. Lett. 26, 207–221.
Staples, R.D., Murphy, D.C., Gibson, H.D., Colpron, M., Berman, R.G., Ryan, J.J., 2014. Middle Jurassic to earliest Cretaceous mid-crustal tectono-metamorphism in the northern Canadian Cordillera: Recording foreland-directed migration of an orogenic front. GSA Bull. 126, 1511–1530.
Staples, R.D., Gibson, H.D., Colpron, M., Ryan, J.J., 2016. An orogenic wedge model for diachronous deformation, metamorphism, and exhumation in the hinterland of the northern Canadian Cordillera. Lithosphere 8, 165–184.
Stern, C.R., 2011. Subduction erosion; rates, mechanisms, and its role in arc magmatism and the evolution of the continental crust and mantle. Gondwana Res. 20 (2–3), 284–308.
Stevens, R.A., Erdmer, P., Creaser, R.A., Grant, S.L., 1996. Mississippian assembly of the Nisutlin assemblage; evidence from primary contact relationships and Mississippian magmatism in the Teslin tectonic zone, part of the Yukon-Tanana Terrane of south-central Yukon. Can. J. Earth Sci. 33 (1), 103–116.
Stolz, A.J., Davies, G.R., Crawford, A.J., Smith, I.E.M., 1993. Sr, Nd and Pb isotopic compositions of calc-alkaline and peralkaline silicic volcanics from the D'Entrecasteaux Islands, Papua New Guinea, and their tectonic significance. Mineral. Petrol. 47 (2–4), 103–126.
Sun, S.S., McDonough, W.F., 1989. chemical and isotopic systematics of oceanic basalts:

implications for mantle composition and processes. In: Saunders, A.D., Norry, M.J. (Eds.), Magmatism in ocean basins 42. Geological Society Special Publication, pp. 313–345.
Taira, A., Mann, P., Rahardiawan, R., 2004. Incipient subduction of the Ontong Java Plateau along the North Solomon Trench. Tectonophysics 389 (3–4), 247–266.
Tani, K., Dunkley, D.J., Ohara, Y., 2011. Termination of backarc spreading; zircon dating of a giant oceanic core complex. Geology 39 (1), 47–50.
Tapster, S., Roberts, N.M.W., Petterson, M.G., Saunders, A.D., Naden, J., 2014. From continent to intra-oceanic arc: zircon xenocrysts record the crustal evolution of the Solomon island arc. Geology 42 (12), 1087–1090.
Taylor, B., Goodliffe, A.M., Martinez, F., 1999. How continents break up; insights from Papua New Guinea. J. Geophys. Res. 104 (B4), 7497–7512.
Tempelman-Kluit, D.J., 1979. Transported cataclasite, ophiolite, and granodiorite in Yukon: evidence of arc-continent collision. Geol. Surv. Can. Pap. 79 (14) (27 p).
Tempelman-Kluit, D.J., Wanless, R.K., 1980. Zircon ages for the Pelly gneiss and Klotassin granodiorite in western Yukon. Can. J. Earth Sci. 17, 297–306.
Tremblay, A., Robertson, A.H.F., Meshi, A., Bedard, J.H., Parlak, O., Koller, F., 2009. Oceanic core complexes and ancient oceanic lithosphere; insights from Iapetan and Tethyan ophiolites (Canada and Albania). Tectonophysics 473 (1–2), 36–52.
Webb, L.E., Baldwin, S.L., Fitzgerald, P.G., 2014. The Early-Middle Miocene subduction complex of the Louisiade Archipelago, southern margin of the Woodlark Rift. Geochem. Geophys. Geosyst. 15. https://doi.org/10.1002/2014GC005500.
Williams, I.S., 1998. U-Pb by ion microprobe. In: McKibben, M.A., Shanks, W.C., Ridley, W.I. (Eds.), Applications of microanalytical techniques to understanding mineralizing processes: Society of Economic Geologists. Rev. Econ. Geol. 7. pp. 1–35.